Available online at www.sciencedirect.com

SCIENCE DIRECT®

Lithos 87 (2006) 104–134

LITHOS

www.elsevier.com/locate/lithos

Interaction between mantle-derived and crustal calc-alkaline magmas in the petrogenesis of the Paleocene Sifton Range volcanic complex, Yukon, Canada

Aleksandar Mišković *, Don Francis

Department of Earth and Planetary Sciences, McGill University, 3450 University Street Montréal, Québec, Canada H3A 2A7

Received 1 May 2004; accepted 25 May 2005
Available online 10 August 2005

Abstract

The uplifted plutons of the eastern Coast Plutonic Complex (CPC) of the northern Canadian Cordillera are in contact with coeval volcanic suites of the early Tertiary Sloko-Skukum Group, offering a unique opportunity to address the relationship between subduction-related, continental calc-alkaline volcanic sequences and their coeval granitoid suites. The Sifton Range volcanic complex (SRVC) of southwestern Yukon is intruded by CPC granites and displays a subduction-related geochemical signature with depletions in HFSE relative to LILE. The volcanic rocks range between medium- and high-K orogenic suites, and define a calc-alkaline fractionation trend. The epizonal potassium–feldspar granites are chemically similar to the SRVC rhyolites, and are characterized by highly fractionated LREE ($La_N/Sm_N = 5–11$), enrichments in LILE and Th (12–18 ppm). The SRVC exhibits a striking relationship between rock composition and style of eruption, with a reduction in abundance of lavas with increasing SiO_2 being correlated with the appearance of felsic pyroclastic rocks and granitic plutonism.

Thermodynamic crystal fractionation models of the compositional interval between basaltic and dacitic andesite (52–61 wt.% SiO_2) are consistent with evolution at moderately hydrous (1.5 wt.% H_2O), upper crustal (1.5 kbar) conditions, and fO_2 close to the QFM buffer. Neither assimilation-fractional crystallization (AFC), nor binary magma mixing models are capable of explaining the anomalously elevated Th contents in the SRVC felsic lavas and granites. Furthermore, unrealistically high contamination factors ($r > 2.5$) are required in AFC models to attain the incompatible-element concentrations of the SRVC granite and rhyolites, suggesting they represent distinct melts derived by anatexis of enriched upper crust, rather than the evolved products of the mafic SRVC magma. Changes in crystallinity during evolution of the SRVC magmas imply an abrupt rise in effective viscosity (from 10^6 to 10^{10} Pa s) near the andesite–dacite transition as a result of the flocculation of plagioclase phenocrysts. The resultant increase in shear strength impeded crystal fractionation and eruption of lavas, and may account for the decrease in the abundance of flows with more than 62 wt.% SiO_2. The onset of explosive volcanism at c.a. 68 wt.% SiO_2 approximately coincides with the calculated saturation point of H_2O at

* Corresponding author. Present address: Département de Minéralogie, Université de Genève, Rue des Maraîchers 13, 1205 Genève, Switzerland. Tel.: +41 22 379 66 36; fax: +41 22 379 32 10.
E-mail address: miskovic@terre.unige.ch (A. Mišković).

0024-4937/$ - see front matter
doi:10.1016/j.lithos.2005.05.007

1.5 kbar in the hybridized dacite magmas. Alternating mafic and felsic volcanic stratigraphy along with the presence of compositionally bimodal pyroclastics and mixed phenocrysts in the SRVC dacites suggest that mantle-derived magmas and crustal melts coexisted in a zoned magmatic column undergoing episodic injection of juvenile melts. Sudden release of volatiles from the hybrid dacitic magmas along the interface with the overlying anatectic crystal mush may have triggered the cycle of explosive eruptions of dominantly rhyolitic ejecta. The consequent loss of volatiles further promoted feldspar crystallization eventually favouring magma stagnation and plutonism.

Keywords: Sifton Range; Calc-alkaline; Volcanism; Plutonism; Canadian Cordillera; Crustal anatexis

1. Introduction

Quantifying the different components that contribute to the petrogenesis of orogenic calc-alkaline magmas remains a difficult task due to their generally evolved compositions and the complexity of pathways exploited by the ascending mantle-derived melts (Green, 1972; Sisson and Grove, 1993; Tatsumi and Eggins, 1995; Kawamoto, 1996; Grove et al., 2003). While crustal melting and assimilation have been shown as effective in producing calc-alkaline differentiation trends in continental arc magmas (Grove et al., 1982; Hildreth and Moorbath, 1988; Tatsumi et al., 2000), debate continues over the relative importance of open- vs. closed-system evolution (Brophy, 1991; Singer et al., 1992). Furthermore, despite numerous surveys of continental calc-alkaline volcanic sequences (Berman, 1981; Druitt and Bacon, 1989; Peccerillo and Wu, 1992; Eichelberger, 1995; Grove et al., 1997) and subduction-related granitoid plutons (Bateman et al., 1963; Bateman and Eaton, 1967; Tepper et al., 1993; Arakawa and Shinmura, 1995), few studies have addressed the relationships between the two. This lacuna is partly a problem of

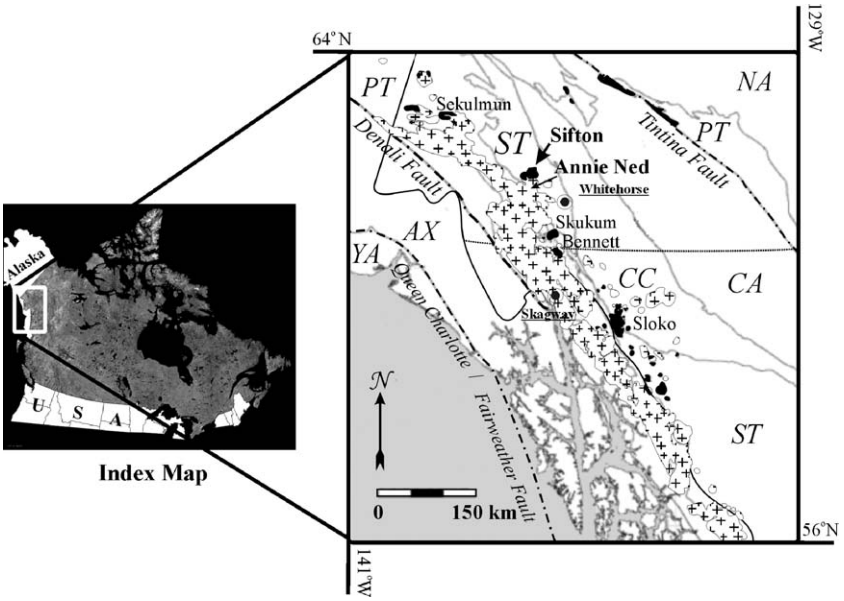

Fig. 1. Tectonic map of the northern Canadian Cordillera showing the Eocene plutons of the Coast Plutonic Complex (crosses), and coeval volcanic remnants of the Sloko-Skukum Group (black). Tectonic terranes: NA—North America, CA—Cassiar, PT—pericratonic terranes (all part of Omineca Belt); CC—Cache Creek, ST—Stikine (Intermontane Belt); AX—Alexander and YA—Yakutat (Insular Belt) (modified after Wheeler and McFeely, 1991).

exposure—where intrusive rocks outcrop, the associated volcanic suite is commonly lost to erosion, whereas preserved volcanic remnants tend to conceal their intrusive counterparts. In the northern Canadian Cordillera however, uplifted batholiths of the Coast Plutonic Complex (CPC) are in direct contact with their contemporaneous volcanic suites and provide an exceptional natural setting for examining this petrogenetic link (Fig. 1).

We report the results of detailed geological mapping and sampling of the Paleocene Sifton Range volcanic complex (SRVC) and the corresponding coeval granitoids of the Nisling Plutonic Suite in the southwestern Yukon. The compositional zoning observed in the SRVC stratigraphy is shown to reflect the coexistence of mantle-derived and crustal anatectic melts in a shallow crustal reservoir. The anomalous enrichment of incompatible trace elements in felsic volcanic rocks and granites of the Sifton Range is explained as resulting primarily from their origin as crustal melts, with the explosive volcanism that accounts for the extensive pyroclastic deposits being related to the saturation of water as fractionating mantle-derived magmas reached dacitic compositions. Finally, we propose a petrogenetic scenario that relates cycles of explosive activity to recharge by juvenile magma, with crustal anatexis producing the felsic lavas and pyroclastics as well as the underlying granites.

2. Tectonic setting

The northern Canadian Cordillera is composed of numerous disparate crustal fragments that were assembled and accreted to the western margin of the North American plate during the Mesozoic (Hart, 1995). The orogen is divided into five morphogeological belts: Foreland, Omineca, Intermontane, Coast Plutonic, and Insular, each comprising a distinctive combination of physiography, lithology, structure, and metamorphic grade (Gabrielse et al., 1991). With an axial length of 1800 km, the Coast Plutonic Belt (Complex; CPC) is the largest exposed continental-margin batholith in the world (Roddick, 1983). It comprises orthogneisses, migmatites, and I-type plutons that were intruded along the western margin of the Intermontane Belt during Mesozoic and early Cenozoic times, and occupies the tectonic suture between dominantly continental arc terranes to the east and ocean arc affinities of the Insular Belt volcanics to the West (Rusmore and Woodsworth, 1991; Monger and Price, 2002). The final phase of widespread plutonism within the CPC occurred during the early Tertiary (62 to 48 Ma), and is linked to a change in motion of the Kula plate relative to the North American craton, from dominantly orthogonal to oblique subduction (Engebretson et al., 1985; Gabrielse and Yorath, 1991). Large-scale contemporaneous uplift of at least 10 km, locally as much as 30 km (Hollister, 1982; Whitney et al., 1999; Valley et al., 2003), was accompanied by erosion that exposed the plutons to increasing depths westward across the northern CPC, resulting in a tonalite–diorite–granite (TDG) transition from the circular granite plutons and alkali–feldspar granitic stocks along the eastern margin of the batholith, through central granodiorites of Ruby Range, Summit Lake, and Clifton (Yukon and British Columbia), to the tonalites of Skagway, Alaska (Barker et al., 1986).

Volcanic activity was pervasive and simultaneous with the plutonism, and remnant volcanic sequences outcrop along the eastern CPC margin and along the length of the Tintina Trench further inboard (Souther, 1991; Fig. 1). In the southern Yukon, major early Tertiary volcanic complexes occur at Sekulmun Lake, Mount Skukum, Bennett Lake, and the Sifton Ranges, and are all assigned to the Skukum Group (Gordey and Makepeace, 1999), whereas in northern British Columbia, equivalent Eocene volcanic rocks outcrop south of Atlin Lake and are referred to as the Sloko Group (Aitken, 1959). Regional mapping by Kindle (1953), Tempelman-Kluit (1974), and Wheeler and McFeely (1991) had variously assigned the Sifton volcanic package to the Triassic Mush Lake Group, to the Middle Cretaceous Mount Nansen Group, and to the Upper Cretaceous Carmacks Group, respectively. Following a reconnaissance survey, the calc-alkaline character of the complex was recognized, and equivalence with the Paleocene Sloko-Skukum Group was proposed (Francis, 2002). The wide compositional spectrum of the Sifton volcanic rocks and their intimate relationship with coeval granitoids make the complex an ideal locality to examine the role of plutonism in the evolution of a continental calc-alkaline volcanic suite.

3. Sifton Range volcanic complex

3.1. Structure and basement

The principal structural feature of the SRVC is a west-northwest-trending half-graben that results in the 10 km-long contact of the Sifton volcanic rocks with the Paleozoic basement southwest of the complex (Fig. 2). Large-scale normal and rotational faulting has locally created offsets in excess of 100 m between corresponding stratigraphic volcanic units. The dominantly southwestern attitudes of bedding planes and the northern orientation of dykes within the SRVC are consistent with dextral northwest transtension being responsible for formation of the graben. The bulk of the Sifton Range volcanic complex is underlain by a green, biotite–muscovite–quartz–feldspar schist, and a more felsic, chlorite–biotite–quartz–feldspar orthogneiss assigned to the pre-Devonian Nisling Assemblage of the Yukon–Tanana Terrane (Tempelman-Kluit, 1974). The early Jurassic Aishihik Suite granodiorites intrude the metamorphic basement, and together with middle Triassic, plagioclase and augite-phyric basalts of Povoas formation, comprise the basement of the SRVC in the western and easternmost sections, respectively.

3.2. Volcanic rocks

Lavas and pyroclastic rocks comprise 40% of the SRVC by area (95 km^2), and total c.a. 65 km^3 of preserved volcanic material. A central granitic stock

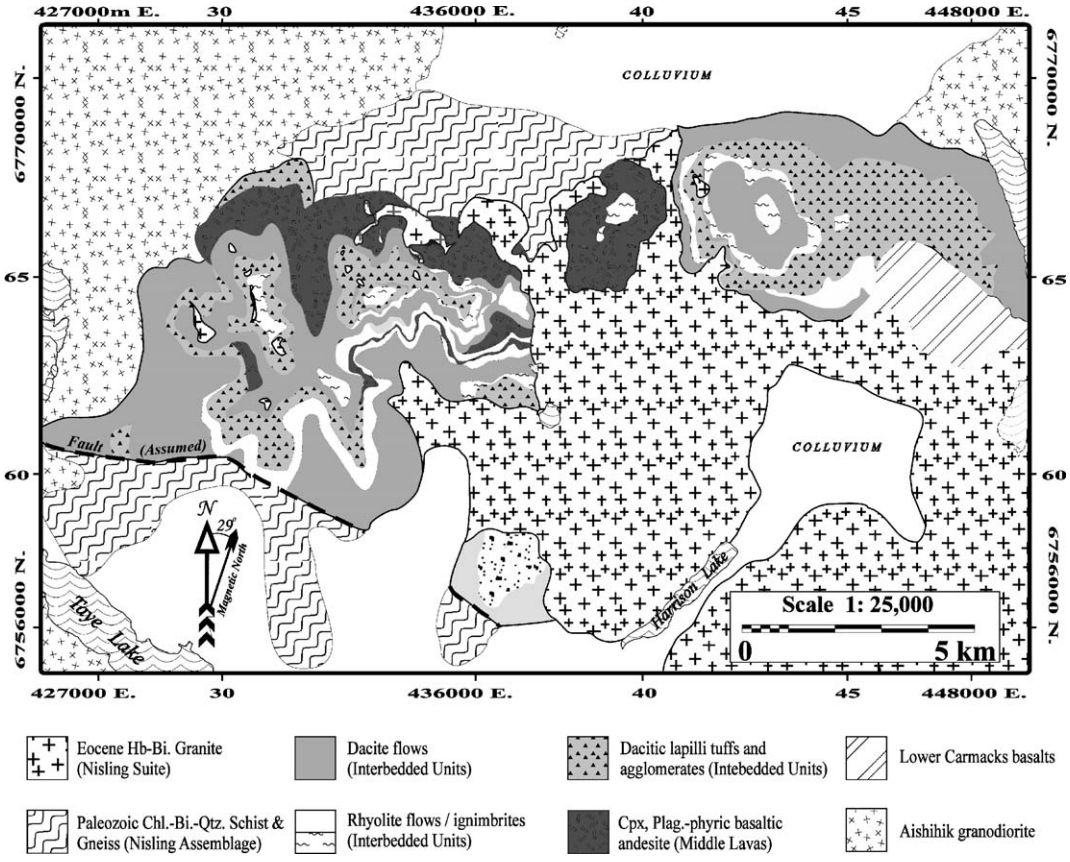

Fig. 2. Simplified geological map of the Sifton Range volcanic complex. Fault contact with the underling metamorphic basement marks the southern extent of the half-graben that served as a depositional trap for the SRVC volcanics. The Lower Interbedded Unit, primarily located in the south, is overlain by the central Middle Lavas and finally, the Upper Interbedded Unit outcropping in the central and northeastern sections of the complex. Monotonous granite intrudes the SRVC from south and southeast, locally tilting the volcanic strata away from the contact.

separates the volcanic pile into larger, dominantly rhyolitic and dacitic segments to the east and west, with relatively primitive basaltic andesites overlying the intrusive plug in the middle of the complex. The volcanic strata are gently inclined to the southwest (5–10°), but the bedding attitudes change locally in the central and western parts of the complex, where rocks dip to the northwest and northeast, away from the intruding granitoids (Fig. 3). Overall, the Sifton volcanic rocks have experienced low-grade, post-depositional alteration characterized by zeolite and sub-greenschist facies mineralogies. The volcanic rocks are subdivided into lava flows, block-and-ash flow tuffs, polymictic breccias (agglomerates), and minor epiclastic deposits. Overall, poorly sorted pyroclastic rocks of variable crystallinity comprise 60% of the eruptive units. Three distinct volcanic sequences are recognized in the SRVC stratigraphy, from bottom to top: (1) the Lower Interbedded Unit, (2) the Middle Lavas, and (3) the Upper Interbedded Unit (Fig. 4).

The Lower Interbedded unit constitutes the bottom 300 m of the exposed volcanic stratigraphy on the southern and easternmost flanks of the complex, in fault contact with the basement. The absolute base of the unit is not exposed. It comprises thick (5–10 m), almost aphyric to feldspar-phyric rhyolitic flows interstratified with dacitic and rhyolitic lapilli tuffs and breccias. Occasional block-and-ash flow deposits form cooling units that are characterized by bimodal clast-size distributions, with andesitic lapilli (2 to 5 cm) and blocks (10 to 30 cm) supported in a monomictic ash and fine lapilli rhyolitic matrix (Fig. 5A). Coarser-grained volcaniclastic rocks near the base of the unit contain abundant fragments of Nisling schist and Aishihik granodioritic basement.

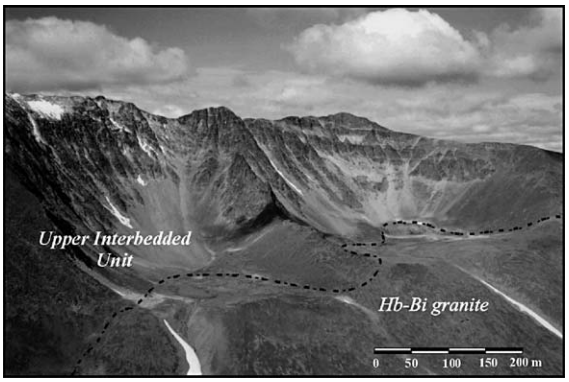

Fig. 3. Westerly view of two cirques carved in gently dipping, interstratified rhyolites and dacitic lapilli tuffs of the SRVC Upper Interbedded. Buff-weathering rocks outcropping in the foreground represent an epizonal granitic intrusion of the Nisling Plutonic Suite. The cirque floors mark the extent of glacial erosion and expose the sharp, intrusive contact (dashed line) between the recessive volcanics and the more competent granitoid basement.

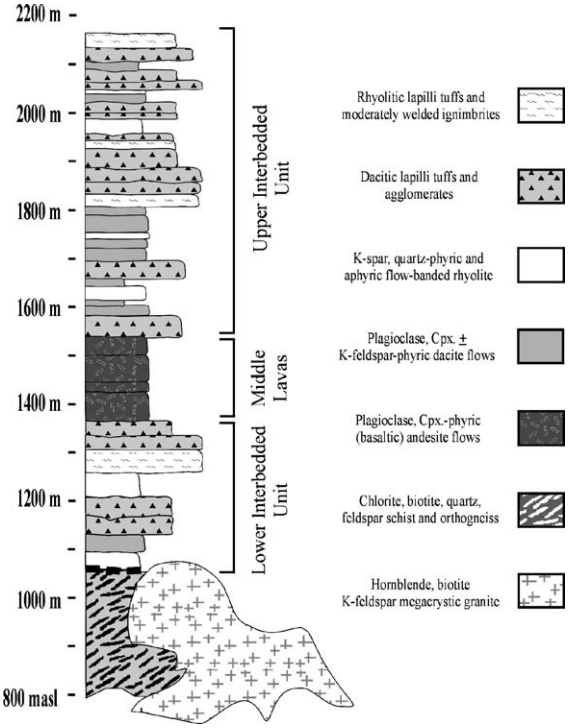

Fig. 4. Composite stratigraphic section for the SRVC. Cyclic pattern of volcanism is recorded in the transition from explosively erupted rhyolitic block-and-ash flows of the Lower Interbedded Unit to effusive outpourings of andesites forming the Middle Lavas and the subsequent reversal to the second episode of pyroclastic-dominated eruption rented by ignimbrites, lapilli and ash tuffs of the Upper Interbedded Unit.

The Middle Lavas comprise a 200 m thick stratigraphic sequence, discontinuously exposed in the central and lowermost stratigraphy of the western part of the complex. This stratigraphic unit is composed of a succession of 5- to 10-m-thick, blue-weathering, sparsely plagioclase-phyric andesite flows overlain by dark grey porphyritic basaltic andesites, where phenocrysts of plagioclase and clinopyroxene occur together with interstitial plagioclase, minor orthopyroxene as well as Fe–Ti oxides.

The Upper Interbedded Unit consists of a sequence of interbedded felsic lavas and pyroclastic cooling

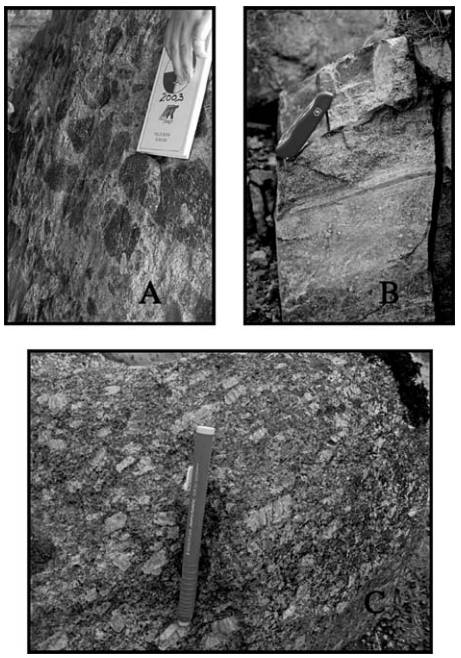

Fig. 5. Representative SRVC rock types: (A) matrix-supported, block-and-ash flow deposits containing abundant plagioclase-phyric andesitic lapilli and blocks set in a rhyolitic ash matrix; (B) finely laminated volcaniclastic siltstone; (C) potassium feldspar megacrysts up to 5 cm long in the biotite, hornblende, two-feldspar granite of the central SRVC.

units, comprising over 550 m of the volcanic succession in the western part of the complex. This segment of stratigraphy is characterized by terraced outcrops formed by the alternation of resistant lapilli tuffs and recessive weathering rhyolite and dacite flows. The bottom 40 m of the unit consists of matrix-supported andesitic lapilli tuffs that are succeeded by a 150-m sequence dominated by 3 to 5-m-thick rhyolite flows, with thin interbeds of green-weathering, epiclastic sandstone and finely laminated ash tuffs. The overlying 150 m consists of a sequence of occasionally welded rhyolitic block-and-ash flows and tephra deposits (Fig. 5B). In general, the pyroclastic rocks of the Upper Interbedded Unit are rhyodacitic in composition, and grade laterally from relatively heterolithic volcanic agglomerates along the eastern and western margins of the complex to thicker lapilli tuffs, and variably crystalline ignimbrite sheets in the centre. In contrast to the compositional homogeneity of the fragmental units of the Lower Interbedded Unit, the pyroclastic rocks of the Upper Interbedded Unit exhibit zoning on a scale of individual cooling units, with coarse-grained, dominantly rhyolitic bottoms, matrix-dominated, rhyodacitic tops, and occasionally densely welded interiors. Within an individual unit, volcanic fragments may change from dominantly andesitic and lesser rhyolitic volcanic blocks up to 50 cm in diameter near the margins to 10-cm-long chloritized, eutaxitic fiammes, and angular lapilli fragments in the center.

3.3. Intrusive rocks

The Sifton Range intrusive rocks define the northernmost extent of the early Tertiary Nisling Range Plutonic Suite, a northwest-trending array of CPC plutons that extends for 230 km from Whitehorse to the northern limit of Kluane Lake. In the SRVC, the plutonic rocks outcrop as a medium-grained, two-feldspar granite that intrudes all three major stratigraphic subdivisions. The SRVC granite is massive, lacking the structural fabric observed in the Mesozoic CPC intrusives (Rusmore and Woodsworth, 1991). It is characterized by distinct plagioclase and potassium feldspars, with the latter forming rare, 4–5 cm long megacrysts exhibiting minor perthitic exsolution textures (Fig. 5C). Mafic phases constitute between 5 and 10 vol.% of the mode, and are dominated by biotite and hornblende, with minor magnetite and clinopyroxene. The SRVC granite does not contain miarolitic cavities observed in other shallow rhyolitic stocks and ring dykes associated with the Sloko-Skukum volcanism in the Bennett Lake and Mt. Skukum complexes (Lambert, 1974; Pride, 1985). Locally, homogeneous volcanic felsites grade into the medium and finally coarse grained granite, but elsewhere in the complex, the contact between the granite and SRVC volcanics is either sharp and irregular, or concealed by volcanic talus.

Dykes and sills are widespread throughout the SRVC, and exhibit a bimodal population. Clinopyroxene and plagioclase-bearing mafic dykes (1–3 m in thickness) indiscriminately cut all the volcanic units, but are noticeably absent within the underlying granite. In contrast, a dense swarm of quartz and feldspar-porphyritic rhyolite dykes radiates from the shallow granite intrusion, particularly in the western part of the complex. In addition, two isolated, sub-angular mafic rafts, 3- to 8-m in diameter were found incorporated deep within the granitic stock. These mafic enclaves do not appear to be roof pendants, and are composed

almost entirely of coarse-grained hornblende with traces of interstitial magnetite and pyrrhotite. A sample of granite collected from the centre of the complex, 300 m below the contact with the SRVC volcanic strata, yielded a concordant U/Pb age on a zircon of 57.5 ± 0.2 Ma (Mortensen, J.K., unpub.). This age is similar to other dates for the Annie Ned pluton to the south and the Nisling Plutonic Suite in general (Hart, 1995), and places a minimum age on the Sifton volcanic package.

Additional plutonic samples were collected across the Annie Ned pluton along the Alaska Highway, 20 km to the south of the Sifton Range. This part of the Nisling Plutonic Suite exhibits a multiphase emplacement history (Hart, 1995), and is more complex in nature than the SRVC granite. Here, early biotite quartz monzogranites and monzodiorites are cut by late leucocratic biotite granites and granodiorites. Both of the intrusive phases are cut by north-trending basaltic dykes (0.5–5 m in thickness), as well as numerous late aplite veins. Locally, the younger granitoids enclose clusters of coarsely crystalline dioritic enclaves that are angular in shape and likely represent remobilized globules of late-stage mafic magma otherwise not observed along the traverse.

4. Geochemistry

4.1. Analytical methods

One hundred and five samples were analyzed for major and selected trace elements (Ba, Co, Cr, Cu, Ni, Sc, V and Zn) by X-ray fluorescence spectrometry at the McGill University Geochemical Laboratories. The samples were jaw crushed, hand picked, ground in an alumina shatter box, and fused into 32 mm-diameter beads prepared from a 1 : 5 mixture of a sample and lithium tetraborate ($B_4Li_2O_7$). Analyses were conducted by a PHILIPS PW2440, 4kW automated XRF spectrometer using α-coefficient technique. Calibration lines are prepared according to 40 international standard reference materials (Govindaraju, 1994). Major-element instrumental precision is within 0.23% relative to stated values, and the overall analytical precision is within 0.5%. The accuracy for SiO_2 is within 0.5%, for other major elements within 1%, and for the selected trace elements within 5% of stated values. Concentrations of Nb, Rb, Sr, Y, and Zr were determined by a combination of α-coefficients and/or Rh-Kp Compton scatter matrix correction using 40 mm-diameter pressed pellets prepared from a mixture of 10 g of sample powder and 2 g of Hoechst Wax C Micro powder. Further standard REE, Ta and Th analyses were performed by a Perkin Elmer ELAN 5000 solution–nebulization inductively coupled plasma mass spectrometer at the University of Saskatchewan. Samples were dissolved in a HF/HNO_3 mixture and spiked with a number of elements according to the analytical protocol of Jenner et al. (1990). Calculated relative analytical error of 3.9% is based on two runs of the QC-standard (BCR-2) and multi-element standards STDA and STDB. Internal monitoring was provided by comparison of Ba, Sr, Rb, Th, Zr, Nb and Y analyses from the two methods.

4.2. Petrography and mineral compositions

Most of the SRVC lavas and pyroclastic rocks are fresh and lack evidence of penetrative deformation. The SRVC lavas display low-pressure, low-temperature mineralogies characteristic of sub-greenschist (zeolite) facies metamorphism, except for the 50- to 100-m-wide contact aureole produced in volcanic rocks along the margins of the pluton, where the phenocrysts and matrix mineralogies tend to be entirely obliterated and the rocks are hornfelsed. In general, alteration is minor and locally evident as plagioclase being partially replaced by secondary epidote, quartz and calcite, as well as augite and rare hornblende phenocrysts being replaced by chlorite. The majority of the SRVC rhyolites, and to a lesser extent dacites, are characterized by hyalocrystalline to cryptocrystalline matrices, while those of the mafic lavas are subtrachytic.

Plagioclase feldspar is the dominant phenocryst in the SRVC lavas, and displays a progressive increase in abundance from 5 vol.% in the basaltic andesites to more than 30 vol.% in evolved andesites near 60 wt.% SiO_2, followed by sharp decline throughout the dacite compositional range (3–10 vol.%) and are absent in the aphyric high-SiO_2 rhyolites. The basaltic andesites and andesites of the SRVC Middle Lavas are characterized by variable plagioclase phenocrysts however, the majority is andesine to labradorite in composition ($An_{43–57}$) and frequently occur together in the same

lava flow with homogeneous phenocrysts of bytownite ($An_{76–80}$), as well as reversely zoned labradorites with rims locally reaching An_{80} (Fig. 6; Table 1). The andesine phenocrysts of the SRVC basaltic andesites are often armored by highly calcic overgrowths (An_{75}), and display corrosion surfaces and skeletal textures indicative of resorption. The dacites of the Interbedded Units also contain a highly heterogeneous population of feldspar phenocrysts. Subhedral, homogeneous, as well as normal and cyclically zoned labradorite and andesine, with An contents oscillating between 50 and 60 mol%, are compositionally similar to those found in the andesites of the Middle Lavas. The SRVC dacites mark the first appearance of anorthoclase feldspar as euhedral, cyclically zoned crystals of restricted compositional range ($Or_{57–61}$). The feldspars of the SRVC granite are distinctly bimodal. Compositions of subhedral plagioclase crystals range from labradorite cores (An_{50}) to andesine rims (An_{31}) with discordant calcic excursions reaching An_{48}. Potassium feldspars of the SRVC granite are megacrystic, also exhibit oscillatory zoning ($Or_{68–Or_{86}}$), and are locally microperthitic with albitic lamellae containing below 10 mol% An (Table 1). Discordant zones in the orthoclase overprint the general trend of decreasing Or content towards the rim.

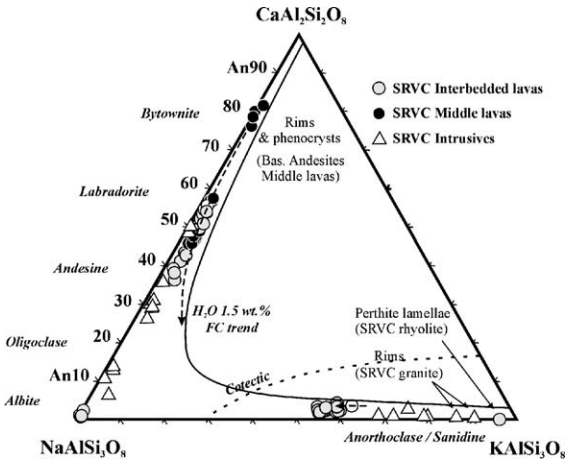

Fig. 6. Feldspar ternary diagram showing the range of compositions from the SRVC. The position of the 1.5 kbar, 900 °C solvus was computed by Solvcalc (Wen and Nekvasil, 1994), according to scheme of Fuhrman and Lindsley (1988). Dark arrowed stippled line indicates compositional trend of fractionating plagioclase as calculated from thermodynamic modeling of whole-rock lava compositions using MELTS (Ghiorso and Sack, 1995).

Pyroxenes are the second most abundant phenocrysts in the SRVC lavas, and occur throughout the compositional range of the volcanic and plutonic rocks. In the andesites of the Middle Lavas, they occur as relatively homogeneous augites ($Wo_{42}En_{43}Fs_{14}$), whereas in the Upper Interbedded dacites (63 wt.% SiO_2), they are reversely zoned, with hedenbergite cores ($Wo_{38}En_{20}Fs_{42}$) evolving to augite rims ($Wo_{40}En_{38}Fs_{22}$), and hosting abundant ilmenite inclusions. Several of the lowermost andesitic dacite flows in the Upper Interbedded Unit contain both reversely zoned clinopyroxenes and subordinate oikocrystic orthopyroxene enclosing plagioclase laths, thus further contributing to the compositional heterogeneity of the phenocryst phases present in the intermediate lavas. Clinopyroxene in the SRVC granites is modally subordinate to hornblende, biotite and opaques whereas, orthopyroxene is absent. Clinopyroxene in the intrusive rocks is euhedral and locally exhibits minor exsolution lamellae of low-Ca pyroxene.

The accessory phenocryst phases in the SRVC lavas include amphibole, quartz, Fe–Ti oxides, and traces of zircon and apatite. Hornblende is conspicuously absent from the SRVC lavas, and appears only in trace amounts as pargasitic relicts in the more evolved dacites of the Upper Interbedded Unit. In contrast to the volcanic rocks, however, hornblende constitutes the most abundant mafic phase of the SRVC granites, and occurs as both euhedral magnesio-hornblende and modally subordinate ferro-hornblende. Ilmenite and Ti-magnetite are primary Fe–Ti oxides in the SRVC volcanic and plutonic rocks, respectively. Magnetite exhibits exsolution lamellae of ilmenite in the basaltic andesites of the SRVC Middle Lavas. The modal proportion of oxides remains constant throughout the compositional range (1–5 vol.%), except for the high-SiO_2 rhyolites which display a sharp increase in abundance of ilmenite relative to the other phenocrysts (up to 15 vol.%; Table 2).

The pyroclastic rocks of the SRVC are predominantly bimodal in composition. The coarser-grained block-and-ash flow deposits are characterized by andesitic to basaltic lapilli fragments and volcanic blocks, up to 25 cm in diameter, incorporated in rhyodacitic matrices (Fig. 5A). Moderately to strongly welded ignimbrites and lapilli tuffs from the central Sifton Range are monomictic, but polycrystalline. Chlori-

Table 1
Mineral chemistry of the SRVC lavas and granites

SRVC SAMPLE	SF-148	SF-148	SF-106	SF-106	SF-106	SF-106	SF-106	SF-135	SF-135	SF-135	SF-135	SF-193	SF-193	SF-193	SF-98	SF-98	SF-98	SF-98	SF-98	SF-98	SF-98
Mineral	Albite	Perthite (host)	Plagioclase (rim)	Plagioclase (inter.)	Plagioclase (core)	Alk. feldspar (rim)	Alk. feldspar (core)	Plagioclase 1	Plagioclase 2	Reversely zoned plagioclase (rim)	Reversely zoned plagioclase (core)	Resorbed plagioclase (rim)	Resorbed plagioclase (core)	Plagioclase 2	Plagioclase (rim)	Plagioclase (inter.)	Plagioclase (inter.)	Plagioclase (core)	K-feldspar (rim)	K-feldspar (inter.)	Albitic lamella
Rock type	High SiO_2 rhyolite	High SiO_2 rhyolite	Dacite	Dacite	Dacite	Dacite	Dacite	Andesite	Andesite	Andesite	Andesite	Andesite	Andesite	Andesite	Granite	Granite	Granite	Granite	Granite	Granite	Granite
Major element chemistry (wt.%)																					
SiO_2	69.02	69.37	56.50	53.84	54.91	65.29	56.64	55.52	57.12	55.78	56.38	56.25	55.75	63.02	62.04	63.17	62.44	62.15	63.56	62.34	68.35
Al_2O_3	19.58	19.62	27.27	28.66	28.27	21.80	26.64	27.99	26.86	27.10	27.41	27.52	27.65	20.89	20.60	20.46	20.71	20.86	19.38	20.27	21.79
FeO	0.02	0.02	0.42	0.60	0.56	0.03	0.42	0.36	0.38	0.39	0.46	0.35	0.49	0.16	0.00	0.00	0.00	0.00	0.00	0.00	0.13
MgO	0.00	0.00	0.06	0.03	0.04	0.00	0.03	0.05	0.05	0.05	0.02	0.04	0.04	0.00	0.01	0.00	0.00	0.00	0.00	0.00	0.00
CaO	0.20	0.19	10.09	11.67	11.12	2.92	9.44	10.83	9.75	10.13	10.05	10.35	10.55	0.69	0.51	0.43	0.61	0.59	0.02	0.20	1.13
Na_2O	11.66	11.57	5.33	4.57	4.93	10.00	5.59	5.07	5.62	5.42	5.41	5.35	5.28	4.15	3.83	4.21	4.05	4.37	1.52	3.26	10.14
K_2O	0.14	0.15	0.51	0.38	0.42	0.08	0.62	0.32	0.43	0.37	0.58	0.34	0.38	9.04	9.84	9.48	9.07	8.75	14.55	10.90	0.79
BaO	0.00	0.00	0.00	0.00	0.00	0.00	0.00	0.00	0.00	0.00	0.00	0.00	0.00	3.16	3.56	3.20	3.57	4.04	0.99	3.49	0.22
Total	100.61	100.93	100.19	99.78	100.26	100.14	99.38	100.15	100.21	99.24	100.31	100.20	100.15	101.30	100.53	101.14	100.60	100.88	100.13	100.59	102.57
Chemistry normalized to 5 cations																					
Si	2.998	3.007	2.548	2.446	2.479	2.880	2.864	2.27	2.56	2.22	2.453	2.598	2.548	2.455	2.708	2.542	2.735	2.517	2.933	2.884	2.943
Al	1.002	1.002	1.449	1.535	1.504	1.125	1.121	1.71	1.43	1.76	1.526	1.388	1.455	1.524	1.281	1.459	1.258	1.479	1.054	1.105	1.106
Fe^{2+}	0.001	0.001	0.016	0.023	0.021	0.006	0.000	0.03	0.02	0.02	0.017	0.016	0.013	0.021	0.008	0.006	0.008	0.006	0.000	0.000	0.005
Mg	0.000	0.000	0.004	0.002	0.002	0.000	0.000	0.00	0.00	0.00	0.002	0.003	0.002	0.004	0.001	0.000	0.001	0.000	0.000	0.000	0.000
Ca	0.009	0.009	0.487	0.568	0.538	0.034	0.025	0.75	0.47	0.80	0.565	0.424	0.475	0.564	0.310	0.481	0.292	0.498	0.001	0.010	0.052
Na	0.982	0.972	0.466	0.403	0.431	0.368	0.343	0.22	0.49	0.19	0.411	0.538	0.485	0.416	0.672	0.502	0.681	0.492	0.136	0.292	0.847
K	0.008	0.008	0.030	0.022	0.024	0.527	0.579	0.02	0.03	0.01	0.024	0.033	0.022	0.016	0.020	0.011	0.025	0.008	0.857	0.643	0.043
Ba	0.000	0.000	0.000	0.000	0.000	0.057	0.064	0.00	0.00	0.00	0.000	0.000	0.000	0.000	0.000	0.000	0.000	0.000	0.018	0.063	0.004
Tot. oxygen	8.005	8.018	8.025	8.002	8.003	7.996	7.964	8.01	8.01	8.00	7.998	8.006	8.022	8.001	8.003	8.015	8.011	8.006	7.964	7.969	8.051
End-member content (mol%)																					
Anorthite	1	1	50	57	54	4	3	76	47	80	57	43	48	57	31	48	29	50	0	1	6
Albite	98	98	47	41	43	40	36	22	49	19	41	54	49	42	67	50	68	49	14	31	90
Orthoclase	1	1	3	2	2	57	61	2	3	1	2	3	2	2	2	1	2	1	86	68	5

Major element chemistry (wt.%)							
SiO_2	41.42	41.47	45.41	45.24	44.81	44.73	46.29
TiO_2	4.29	4.19	1.63	1.71	1.72	1.63	1.34
Al_2O_3	11.68	11.48	7.12	7.58	7.57	7.55	6.50
Cr_2O_3	0.02	0.03	0.00	0.00	0.01	0.01	0.00
FeO	11.70	12.17	17.98	18.14	18.39	18.84	18.07
MgO	13.96	13.81	11.16	10.92	10.53	10.09	11.12
MnO	0.16	0.18	0.97	0.88	1.08	1.19	1.03
CaO	11.14	11.37	10.95	10.95	10.85	10.70	10.64
Na_2O	2.464	2.46	1.75	1.81	1.81	1.82	1.81
K_2O	0.98	1.03	0.83	0.89	0.87	0.88	0.68
F	0.40	0.51	0.77	0.69	0.43	0.58	0.75
Cl	0.01	0.03	0.06	0.10	0.10	0.10	0.08
Total	98.04	98.51	98.30	98.60	97.96	97.87	97.99
H_2O (calculated)	1.96	1.49	1.71	1.40	2.04	2.13	2.01
IMA name	Pargasite	Pargasite	Mg-hornblende	Mg-hornblende	Mg-hornblende	Fe-hornblende	Mg-hornblende
Chemistry normalized to 15 cations (all Na and K confined to A site)							
Si	6.121	6.125	6.857	6.814	6.802	6.819	6.993
Al (iv)	1.879	1.875	1.143	1.186	1.198	1.181	1.007
T site	8.000	8.000	8.000	8.000	8.000	8.000	8.000
Al (vi)	0.155	0.123	0.125	0.160	0.157	0.176	0.151
Ti	0.477	0.465	0.185	0.193	0.196	0.187	0.152
Cr	0.002	0.004	0.000	0.000	0.001	0.001	0.000
Fe^{3+}	0.000	0.000	0.000	0.000	0.000	0.000	0.000
Fe^{2+}	1.446	1.503	2.270	2.284	2.333	2.402	2.283
Mn	0.020	0.023	0.124	0.113	0.139	0.154	0.132
Mg	3.075	3.041	2.512	2.452	2.383	2.293	2.504
Ca	1.763	1.798	1.772	1.766	1.765	1.748	1.722
C+B sites	6.939	6.959	6.988	6.970	6.974	6.960	6.945
Na	0.706	0.705	0.511	0.529	0.531	0.539	0.530
K	0.185	0.193	0.160	0.171	0.169	0.172	0.131
A site	0.891	0.899	0.672	0.700	0.700	0.710	0.661

(continued on next page)

Table 1 (*continued*)

SRVC sample	SF-106	SF-106	SF-106	SF-106	SF-139	SF-139	SF-139
Mineral	Clinopyroxene (rim)	Clinopyroxene (inter.)	Clinopyroxene (inter.)	Clinopyroxene (core)	Clinopyroxene 1	Clinopyroxene 2	Clinopyroxene 3
Rock type	Dacite	Dacite	Dacite	Dacite	Dacite	Dacite	Dacite
Major element chemistry (wt.%)							
SiO_2	51.49	50.86	50.58	50.07	51.99	51.91	51.89
TiO_2	0.41	0.30	0.17	0.19	0.38	0.43	0.37
Al_2O_3	1.28	0.61	0.67	0.75	1.32	1.45	1.47
FeO	10.18	15.26	17.74	18.96	6.96	6.75	6.93
Fe_2O_3	2.15	2.18	2.18	1.76	2.18	1.99	2.05
Cr_2O_3	0.01	0.00	0.01	0.00	0.02	0.01	0.02
MnO	0.53	0.80	0.96	1.06	0.34	0.32	0.39
MgO	14.41	10.23	8.50	7.95	15.19	15.34	15.28
CaO	19.17	19.95	19.77	19.19	20.98	21.03	20.84
Na_2O	0.28	0.32	0.36	0.40	0.38	0.32	0.34
Total	99.93	100.49	100.94	100.23	99.74	99.56	99.58
Mg #	70	53	45	42	77	78	78
Ca/Na	68	62	55	48	55	66	61
Chemistry normalized to 4 cations							
Si	1.949	1.970	1.974	1.973	1.950	1.947	1.948
Ti	0.012	0.009	0.005	0.006	0.011	0.012	0.010
Al	0.057	0.028	0.031	0.035	0.058	0.064	0.065
Fe^{2+}	0.322	0.494	0.579	0.625	0.218	0.212	0.217
Fe^{3+}	0.031	0.032	0.032	0.026	0.031	0.028	0.029
Cr	0.000	0.000	0.000	0.000	0.000	0.000	0.000
Mn	0.017	0.026	0.032	0.035	0.011	0.010	0.012
Mg	0.813	0.591	0.494	0.467	0.849	0.858	0.855
Ca	0.778	0.827	0.826	0.810	0.843	0.845	0.838
Na	0.021	0.024	0.027	0.022	0.027	0.024	0.024
Total oxygen	5.979	5.980	5.980	5.985	5.976	5.979	5.978
End-member content (mol%)							
Wo	40	41	41	39	42	42	42
En	40	29	24	23	42	43	43
Fs	20	29	33	35	14	14	14
Ac	1	1	1	1	1	1	1

Selected microprobe analyses of feldspar and clinopyroxenes in SRVC lavas and granites. Mineral analyses were conducted on a JEOL 8900 Super probe at the McGill University Microprobe Laboratory using ZAF correction method, 15 kV accelerating voltage, and 20 nA beam current. Beam size was adjusted depending on grain sizes and varied between 2 and 5 çm. The counting time for most elements was 20 s on the peak emission and 20 s on the background (for Cl, counting time was 30 s on peak intensities and 30 s on background). Standardized natural and synthetic minerals are used for calibration. Ferric iron was recalculated after procedure of Droop (1987), assuming full site occupancy.

tized mafic fiamme occur together with volumetrically minor anhedral quartz, plagioclase, and potassium feldspar and are surrounded by glassy to devitrified rhyolitic matrix. Reworked pyroclastic deposits are differentiated from primary ones based on their enrichment in lithic fragments derived from diverse sources, including pieces of the basement Aishihik granodiorite (up to 25 vol.%).

Table 2
Measured SRVC lava crystallinities and modeled fractionated solid assemblage (MELTS)

SRVC sample	SiO_2 (wt.%)	Cpx (%)	Opx (%)	Feld. (%)	Hbd. (%)	Opaques (%)	Qtz. ± Acces. (%)	Total crystallinity (vol.%)
SF-136	53.2	85		10		5		6.0
SF-135	56.3	25	10	60		5		8.5
SF-139	59.5	35	10	45	5	5		12.1
SF-156	59.8	5	5	80		10		15.6
SF-161	60.0		15	75	5	5		20.7
SF-167	60.1		10	80		10		18.8
SF-109	60.5	5		80	10	5		30.6
SF-152	61.0	5	15	75		5		18.1
SF-193	61.3	30	5	60		5		7.5
SF-219b	62.0	5	10	80	5			7.0
SF-80	62.1	10	5	80		5		3.2
SF-191	62.8		5	95				2.2
SF-106	63.4	35		60	5			3.2
SF-153	63.7	5	5	80		5	5	13.9
SF-185	66.0			90		5	5	6.2
SF-119	66.1		5	80		10	5	15.1
SF-195	66.4			80		15	5	5.8
SF-189	68.2			75		5	20	5.0
SF-142	68.7			65		10	25	7.5
SF-128	69.9			60		10	30	8.0
SF-81	70.5			60			40	10.0
SF-77	72.1	5	5	60		10	20	7.7
SF-148	74.0			65	5		30	3.4
SF-82	75.0			55		5	40	1.8

MELTS phases crystallized (1.5 kbar, 1.5 wt.% H_2O initial)	SiO_2 (wt.%)	Ol. (%)	Cpx (%)	Opx (%)	Feld. (%)	Fe–Ti oxide ± spinel	Apatite	Total crystallized (vol.%)
Ol.	53.68	100						1.0
Ol.	53.91	100						3.0
Cpx, spin.	54.13	95				5		4.0
Opx, spin, cpx	54.25		30	65		5		5.0
Spin, cpx	54.57		90			10		9.5
Spin., cpx, plag.	54.76		25		70	5		12.0
High-Ca cpx, low –Ca cpx, plag.	55.28		30		70			19.0
High-Ca cpx, low –Ca cpx, plag.	56.39		30		70			32.0
Opx, high-Ca cpx, low-Ca cpx, plag.	57.25		10	15	75			37.5
Opx, plag.	58.80			15	85			40.5
Cpx, plag.	61.36		20		80			53.0
Cpx, plag.	62.50		15		85			57.0
Cpx, plag., opx	64.07		15	5	80			61.4
Cpx, plag., K-spar. + H_2O	65.39		10		90			64.0
Cpx, plag., K-spar., Fe–Ti ox. + H_2O	66.60		5		80	15		69.7
Plag., K-spar., Fe–Ti ox., apat. + H_2O	67.34				75	20	5	73.0

Modal abundances of plagioclase phenocrysts observed in 23 SRVC lavas ranging from andesite to high-silica rhyolite. Crystallinity was determined by threshold-sensitive morphometry in Northern Eclipse 4.0 program. Also shown are phases and volumetric proportions of fractionated mineral assemblage in MELTS program (Ghiorso and Sack, 1995) at 1.5 kbar and initial magma H_2O content of 1.5 wt.%.

Table 3
SRVC whole-rock major and trace element chemistry including CIPW normative mineralogy

Sample	SF-148	SF-77	SF-81	SF-195	SF-106	SF-72	SF-123	SF-135	SF-138	SF-261
Unit/location	Upper Interbedded unit	Lower Interbedded unit	Upper Interbedded lavas	Upper Interbedded unit	Upper Interbedded unit	Middle lavas	Middle lavas	Middle lavas	Middle lavas	Middle lavas
Rock type	High SiO_2 rhyolite	Rhyolite	Rhyolite	Dacite	Dacite	Andesite	Andesite	Andesite	Bas. Andesite	Bas. Andesite
Normalized elevation (m)	1630	1220	1960	1800	1590	1368	1430	1490	1510	1540
Major element chemistry (wt.%) Fe^{+3} = Fe tot.										
SiO_2	74.0	72.9	70.5	66.4	63.4	55.8	56.3	56.3	53.5	53.9
TiO_2	0.23	0.19	0.31	0.54	0.86	1.30	1.30	1.17	1.41	1.36
Al_2O_3	14.1	14.0	13.9	16.6	16.2	15.5	16.5	18.4	17.0	16.4
Fe_2O_3	1.46	1.63	3.56	3.73	5.99	8.39	8.90	8.03	9.74	9.22
MnO	0.01	0.05	0.10	0.10	0.13	0.14	0.10	0.16	0.18	0.15
MgO	0.34	0.05	0.35	0.68	0.76	5.50	3.90	2.79	4.31	4.32
CaO	0.23	1.30	1.38	1.98	3.75	7.78	6.31	6.76	8.06	8.22
Na_2O	6.56	3.47	3.35	4.68	4.60	2.82	4.05	3.92	3.38	3.84
K_2O	2.10	4.84	4.40	4.29	3.11	1.32	1.20	2.20	1.53	1.47
P_2O_5	0.05	0.05	0.08	0.12	0.30	0.36	0.34	0.37	0.56	0.53
LOI	0.54	1.58	1.83	0.53	0.68	1.46	1.63	0.38	0.69	0.79
Total	99.70	100.00	99.68	99.65	99.71	100.37	100.53	100.52	100.38	100.18
Mg #	19	3	9	15	11	40	30	26	31	32
Trace elements (ppm)										
Cu	6	9	7	39	0	153	13	17	52	0
Zn	0	2	14	108	0	23	64	72	92	0
Cr	22	8	23	9	0	291	200	0	194	205
Ni	3	4	0	2	0	66	13	0	35	36
V	14	13	19	11	0	136	162	154	165	151
Co	7	2	6	3	0	30	4	15	30	28
Y	14	16	39	35	34	31	27	35	28	26
Nb	22	9	11	16	15	6	7	<0.3	4	4
Zr	164	183	281	258	281	148	177	173	208	197
Sr	74	254	158	358	458	406	494	557	736	729
Rb	57	159	122	111	92	61	34	63	48	42
Ba	471	1802	1870	2304	0	551	1179	1379	1236	1692
Ga	16	15	16	15	18	19	20	23	22	20
Ta	<2	<2	<2	<2	<2	<2	<2	<2	<2	<2
Th	14	19	11	12	8	9	5	3	3	3
U	5	5	5	4	<1	4	4	4	3	3
Pb	4	22	16	11	17	7	8	6	8	12
CIPW normative mineralogy (wt.%) Fe^{+3}/Fe_{total} = 0.2										
Quartz	26.6	31.0	29.7	16.1	14.4	9.4	7.3	5.0	3.6	2.4
Orthoclase	12.5	29.1	26.6	25.6	18.6	7.9	7.2	13.1	9.1	8.8
Plagioclase (total)	56.9	36.5	35.9	49.7	54.0	50.3	58.5	59.6	56.0	56.2
Albite	56.0	29.8	29.0	40.0	39.5	24.3	34.9	33.3	28.9	32.9
Anorthite	0.9	6.7	6.9	9.7	14.5	26.1	23.6	26.3	27.1	23.3
Clinopyroxene	0.0	0.0	0.0	0.0	2.2	9.0	5.3	4.5	8.3	12.4
Diopside	0.0	0.0	0.0	0.0	0.6	6.0	3.0	2.3	4.8	7.3
Hedenbergite	0.0	0.0	0.0	0.0	1.6	3.0	2.2	2.2	3.6	5.1
Orthopyroxene	2.2	1.8	4.8	5.4	6.7	17.5	15.7	12.4	16.1	13.6
Enstatite	0.9	0.1	0.9	1.7	1.6	11.1	8.5	5.9	8.6	7.5
Ferrosilite	1.3	1.7	3.9	3.7	5.0	6.4	7.3	6.5	7.5	6.1
Olivine	0.0	0.0	0.0	0.0	0.0	0.0	0.0	0.0	0.0	0.0
Chromite	0.0	0.0	0.0	0.0	0.0	0.1	0.0	0.0	0.0	0.0
Magnetite	0.4	0.5	1.1	1.1	1.8	2.5	2.6	2.3	2.9	2.7
Ilmenite	0.5	0.4	0.6	1.0	1.7	2.5	2.5	2.2	2.7	2.6
Apatite	0.1	0.1	0.2	0.3	0.7	0.8	0.8	0.8	1.2	1.2
Zircon	0.0	0.0	0.1	0.1	0.1	0.0	0.0	0.0	0.0	0.0

Table 3 (*continued*)

Sample	SF-60	SF-61	SF-63	SF-64	SF-98
Unit/location	Sifton Range plutonic	Sifton Range plutonic	Sifton Range plutonic	Sifton Range plutonic	Sifton Range plutonic
Rock type (IUGS)	Granite	Granite	Alk. feld. granite	Alk. feld. granite	Granite
Elevation (m)	1776	1738	1655	1594	1470
Major element chemistry (wt.%) Fe^{+3}= Fe tot.					
SiO_2	69.7	69.9	70.5	69.7	69.8
TiO_2	0.36	0.36	0.30	0.36	0.39
Al_2O_3	14.6	14.6	14.6	14.5	15.0
Fe_2O_3	2.6	2.64	2.30	2.53	2.66
MnO	0.12	0.08	0.11	0.07	0.11
MgO	0.71	0.71	0.50	0.64	0.66
CaO	1.74	1.68	1.00	1.57	1.96
Na_2O	4.03	3.93	4.42	3.63	4.13
K_2O	4.63	4.62	4.96	4.86	4.40
P_2O_5	0.1	0.1	0.08	0.10	0.13
LOI	1.38	1.13	1.19	1.57	0.6
Total	99.97	99.70	99.96	99.59	99.84
Molar A/CNK	0.86	0.88	0.84	0.88	0.89
Trace elements (ppm)					
Cu	44	5	9	10	7
Zn	37	27	29	10	17
Cr	15	21	9	21	11
Ni	13	3	2	3	1
V	27	35	22	32	29
Co	4	8	2	10	3
Y	28	25	31	25	23
Nb	11	9	10	7	9
Zr	223	225	244	239	206
Sr	213	230	175	271	299
Rb	129	149	139	168	154
Ba	2299	2370	2722	2737	2183
Ga	17	17	16	16	16
Ta	<2	<2	<2	<2	<2
Th	15	17	13	23	12
U	5	5	5	5	5
Pb	16	16	10	16	16
CIPW normative mineralogy (wt.%) Fe^{+3}/Fe_{total}= 0.2					
Quartz	23.1	23.9	22.8	25.1	22.9
Orthoclase	27.8	27.7	29.8	29.3	26.2
Plagioclase (total)	42.7	42.1	43.2	39.3	44.7
Albite	34.6	33.8	38.0	31.4	35.2
Anorthite	8.1	8.4	5.1	7.9	9.5
Clinopyroxene	0.5	0.0	0.0	0.0	0.0
Diopside	0.2	0.0	0.0	0.0	0.0
Hedenbergite	0.3	0.0	0.0	0.0	0.0
Orthopyroxene	4.2	4.4	2.6	4.1	4.3
Enstatite	1.7	1.8	0.2	1.6	1.7
Ferrosilite	2.6	2.7	2.4	2.5	2.7
Olivine	0.0	0.0	0.0	0.0	0.0
Chromite	0.0	0.0	0.0	0.0	0.0
Magnetite	0.8	0.8	0.7	0.8	0.8
Ilmenite	0.7	0.7	0.6	0.7	0.8
Apatite	0.2	0.2	0.2	0.2	0.3
Zircon	0.1	0.1	0.1	0.1	0.0

Selected major and trace element chemistry of the SRVC rocks with the CIPW normative mineralogy.

4.3. Whole-rock chemistry

All the SRVC lavas are silica oversaturated (Table 3). The volcanics span a compositional continuum from basaltic andesite (52 wt.% SiO_2) to high-SiO_2 rhyolites (72 wt.% SiO_2), with a prominent population mode near the andesite–dacite transition (Fig. 7). Analyses of homogeneous matrices from the SRVC lapilli tuffs and moderately welded ignimbrites indicate rhyolitic compositions similar to the SRVC rhyolites (68–70 wt.% SiO_2), but display elevated Ba (2000–2200 ppm) and Th contents (10–12 ppm Th). The SRVC lavas cross the traditional boundary between medium- and high-K orogenic suites in the K_2O vs. SiO_2 classification scheme of Gill (1981), with the bulk of the felsic lavas and intrusive rocks falling in the high-K field (Fig. 8A). This transition is associated with a population minimum in the range between 56 and 59 wt.% SiO_2. A decrease in abundance of more felsic lavas with increasing SiO_2 is associated with the increase in volume of pyroclastic rocks, as well as the emplacement of granite. Together, the SRVC volcanic and intrusive rocks define a calc-alkaline differentiation trend in terms of continuously decreasing TiO_2 with increasing FeO*/MgO (Miyashiro, 1974), and lack the Fe-enrichment that is characteristic of tholeiitic suites (Fig. 8B). The whole-rock Fe/Mg ratios indicate that the most primitive SRVC members could not have coexisted with mantle olivines (i.e. $Fo_{90–92}$) and therefore must represent moderately modified liquids.

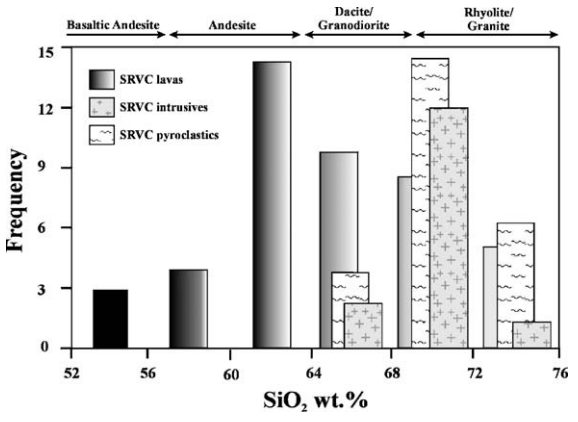

Fig. 7. Sample frequency (volumetric proportion) vs. SiO_2 histogram showing the relationship between the composition of the SRVC volcanic and plutonic rocks. Sampling was conducted on a sample per flow/cooling unit basis along six vertical traverses through the volcano-stratigraphic column.

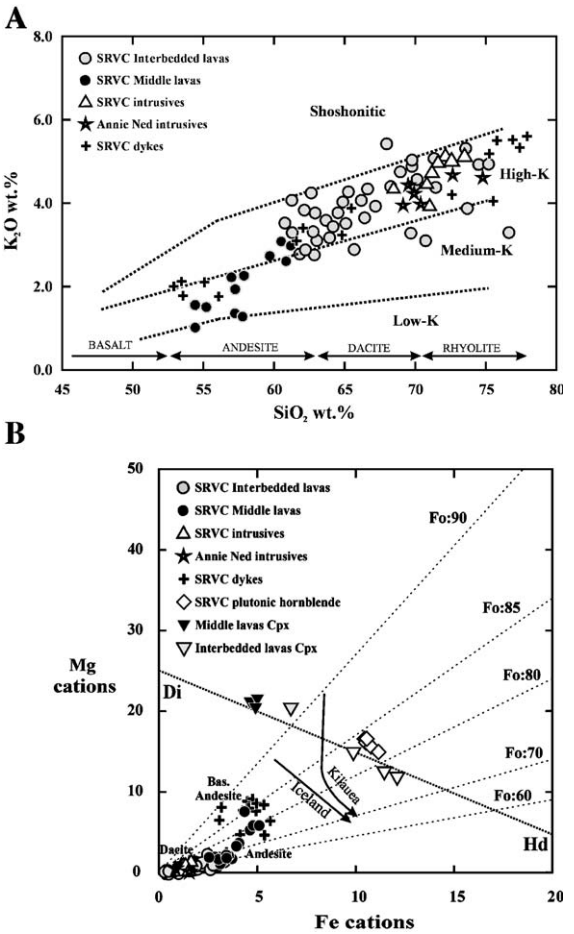

Fig. 8. (A) SRVC lavas and intrusive rocks in a K_2O vs. SiO_2 diagram with Gill's (1981) classification scheme for orogenic magmas. (B) The SRVC lavas, dykes, and plutons on an Mg vs. Fe plot in cation units ($Fe^{+3}/Fe_{tot.}=0.2$ assuming QFM conditions). Dashed lines indicate the compositions of coexisting olivine assuming an Fe–Mg partition coefficient between olivine and a silicate liquid of 0.33. Also shown is the diopside–hedenbergite compositional line with clinopyroxene phenocrysts from the SRVC lavas. Iceland and Kilauea tholeiitic trends derived from Sigmarsson et al. (1992), and Clague and Dalrymple (1987), respectively.

The SRVC plutonic samples straddle the border between the granite and alkali-feldspar granite in the standard IUGS classification of Le Maitre (1989). The samples of the Annie Ned pluton, on the other hand, exhibit a much wider compositional range with the older quartz monzodiorites and alkali-feldspar sye-

nites being intruded by younger granitic pulses. The SRVC metaluminous granites (A/CNK 0.86–0.89) and the felsic lavas define linear arrays that are offset from the H_2O-saturated cotectics toward the primary phase field of orthoclase in the Ab–Or–Qtz–H_2O pseudoternary system of Tuttle and Bowen (1958; Fig. 9). Granitoid rocks of the Annie Ned pluton have lower normative quartz and fall closer to the 5 kbar water-saturated ternary eutectic in the haplogranite system.

The progression from the SRVC basaltic andesite to rhyolite is accompanied by a continuous increase in LILE, LREE, and most HFSE, except for P and Sr which systematically decrease through the compositional range. A decrease in Ba, Y and Zr beyond 70 wt.% SiO_2 can be attributed to appearance of phases with high partition coefficients for these elements; potassium feldspar, hornblende, and zircon (apatite), respectively. The trace element content of the SRVC

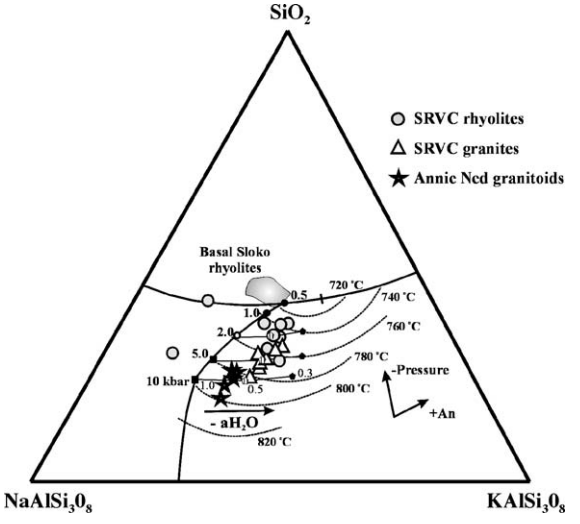

Fig. 9. Normative mineralogy of the SRVC rhyolites and intrusives, Annie Ned granitoids and rhyolite lavas from the Sloko Lake volcanic complex of northern British Columbia (Resnick, 2003) projected in the experimentally determined (Ca-free) Quartz–Albite–Orthoclase–H_2O pseudoternary diagram of Tuttle and Bowen (1958). Black squares and circles indicate positions of water-saturated ternary eutectics and minima, respectively, at given H_2O pressures. Temperature contours from 1 kbar H_2O-saturated experiments of Carmichael and MacKenzie (1963). Arrows show the effects of increasing An content, lowering of pressure and decreasing water activities due to elevated F^- and Cl^- in the residual melt.

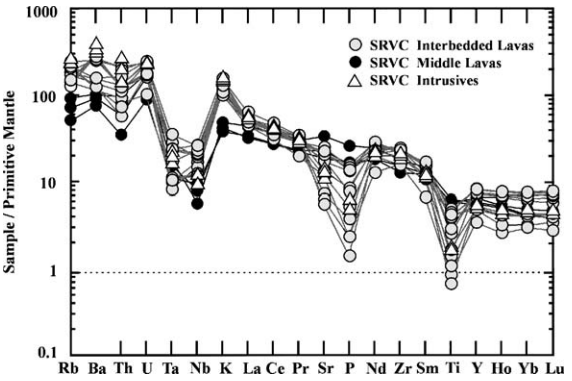

Fig. 10. Primitive mantle (PM) normalized trace element diagram for SRVC rocks (PM values from McDonough and Sun, 1995). The SRVC rocks display unfractionated HREE, elevated LILE, and prominent Ti, P and Ta–Nb anomalies.

granite is identical to slightly elevated with respect to the felsic lavas of the equivalent SiO_2 content. In particular, the granite is characterized by enrichments in LILE content (Ba, Rb and K), as well as the highly incompatible elements Th (12–18 ppm) and Pb (15–20 ppm). Compatible trace element abundances are low throughout the SRVC suite (<10 ppm Ni; <50 ppm Cr), with only three basaltic andesites of the Middle Lavas having values higher than 35 ppm Ni and 180 ppm Cr. Primitive mantle normalized trace element patterns for the SRVC volcanic and plutonic rocks are characteristics of subduction-related magmas, with relative depletions in high field strength elements (Ti, P, Ta and Nb) and prominent enrichments in thorium, uranium and LILE (K, Rb and Ba; Fig. 10). Both the plutonic and volcanic rocks display sub-parallel REE patterns characterized by relatively flat HREE, but fractionated LREE $(La/Sm)_N = 5–11$, particularly in the felsic lavas and granites, and show mild negative Eu anomalies $(Eu/Eu^* = 0.4–1.0)$.

5. Discussion

The SRVC volcanic stratigraphy displays two contrasting magma types. The volumetrically minor and relatively primitive basaltic andesites of the Middle Lavas are bracketed in time by the trace element enriched dacites, rhyolites and the compositionally equivalent pyroclastic of the Interbedded Units. This

package was then intruded by granites that are chemically indistinguishable from the SRVC felsic volcanics. These intimate field relationships, combined with the correlation between composition and style of eruption or emplacement appear to reflect the interaction between mantle-derived melts and the crust of the northern Coast Plutonic Complex of the Canadian Cordillera.

5.1. Source of parental magmas

Although the least fractionated basaltic andesite flows of the Middle Lavas contain only up to 5.5 wt.% MgO (Table 3 and 4), higher-MgO compositions (MgO > 8.0 wt.%) have been documented in other early Tertiary volcanic suites of the northern Cordillera, including Sloko Lake, and the Hoole and White

Table 4
AFC and EC-RAFC parameters used for modeling upper crustal assimilation

Material	Parental dyke (magma)	Upper crust assimilant
Unit/location	SF-136 SRVC	SF-77 SRVC
Rock type (IUGS)	Basaltic andesite	High-SiO_2 rhyolite
Major element chemistry (wt.%) Fe^{+3} = *Fe tot.*		
SiO_2	52.6	72.9
TiO_2	1.30	0.19
Al_2O_3	15.4	14.0
Fe_2O_3	8.85	1.63
MnO	0.18	0.05
MgO	6.61	0.05
CaO	8.02	1.30
Na_2O	2.66	3.47
K_2O	1.98	4.84
P_2O_5	0.35	0.05
LOI	2.39	1.88
Total	100.34	100.30
Th (ppm)	1.7	18.6
Bulk D_{Th}	0.1728	0.2157

Assimilation parameters	EC-AFC step 2 MgO < 1.79 wt.% (preheated upper crust)	Xstaln step 2 MgO < 1.79 wt.% (preheated upper crust)	Xstaln step 3 MgO < 0.82 wt.% (preheated upper crust)
Magma liquidus temperature (°C)	1219	1219	1219
Initial magma temperature (°C)	1060	1219	1219
Assimilant liquidus temperature (°C)	900	900	900
Initial assimilant temperature (°C)	300	900	900
Solidus temperature (°C)	810	810	810
Equilibration temperature (°C)	885	–	–
Specific heat capacity of magma (kJ/kg K)	1.484	–	–
Specific heat capacity of assimilant (kJ/kg K)	1.200	–	–
Latent heat of crystallization of magma (kJ/kg)	350	–	–
Latent heat of fusion of assimilant (kJ/kg)	200	–	–
Total mass of assimilated rock (% relative to initial magma mass)	26	32.6	161
Total mass of cumulates formed (% relative to initial magma mass)	46	34.2	56.9
Ratio of assimilated wallrock to cumulates formed (DePaolo's assimilation coefficient *r*)	0.57	0.95	2.83

Assimilation fractional crystallization (AFC) and Energy-Constrained Assimilation Fractional Crystallization (Bohrson and Spera, 2001) parameters used in modeling upper crustal (1.52 kbar) assimilation by magma recharge during the SRVC petrogenesis.

River localities (Resnick, 2003; Pride, 1988; Hasik, 1994). The concentrations of HFSE are commonly used to characterize the mantle source region of subduction-related basalts because of their low mobility during hydrous fluxing of the mantle wedge and their overall chemical inertness (Bailey and Ragnasdottir, 1994). The abundance of these elements in arc magmas is thought to be primarily a reflection of the degree of partial melting, and the overall composition of the source. The SRVC basaltic andesites are characterized by HFSE ratios that are enriched relative to the N-MORB mantle source (Fig. 11A), and their unfractionated HREE patterns are consistent with genesis, or last equilibration with the mantle in the spinel lherzolite facies at pressures below 20 kbar. Although the relatively primitive SRVC lavas exhibit similar mantle-normalized HFSE ratios relative to basalts of the other early Tertiary suites, they have relatively high contents of Th (up to 9 ppm), and display larger negative Ta–Nb anomalies (Fig. 11B). This distinctive signature of the SRVC magmas does not appear to be a function of their lower MgO content (i.e. degree of fractionation), because it also holds when compared to Mt. Skukum and Bennett Lake lavas with equivalent or even lower MgO contents (3.2–4.0 wt.%; Morris and Creaser, 2003).

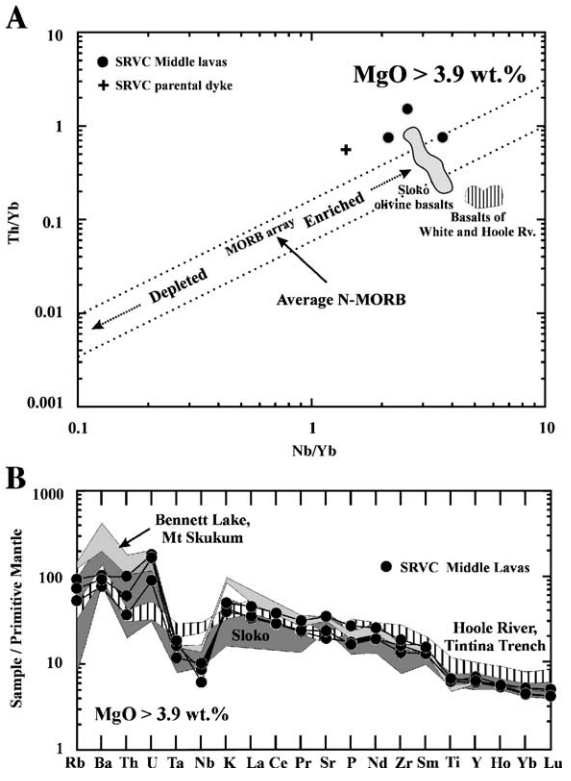

Fig. 11. (A) Th/Yb vs. Nb/Yb source plot for the SRVC (basaltic) andesites compared to primitive lavas of the early Tertiary volcanic centres in the northern Canadian Cordillera (modified after Pearce and Peate, 1995). (B) Primitive mantle normalized trace element diagram for the SRVC (basaltic) andesites compared to those found in the other early Tertiary volcanic centres (normalizing values from McDonough and Sun, 1995).

5.2. Major and trace element modeling

The compositional trends of the SRVC lavas can be modeled in terms of the effects of variable water content on the saturation of plagioclase and ilmenite during crystal fractionation. Elevated water concentration (>2–3 wt.%) tends to suppress the appearance of plagioclase on the liquidus (Spulber and Rutherford, 1983; Baker and Eggler, 1987), and if hydrogen can effectively diffuse away from reaction sites, also promotes the early precipitation of Fe–Ti oxide phases due to increased oxygen fugacity and the associated oxidization of ferrous to ferric iron (Frost and Lindsley, 1992; Brandon and Draper, 1998). In order to account for the major and trace element variability of the SRVC lavas and intrusive rocks, we investigated the effects of pressure, temperature, fO_2, and H_2O content during crystal fractionation of the SRVC magmas. Three petrogenetic scenarios were considered: (1) closed-system fractional crystallization, (2) assimilation-fractional crystallization (AFC), and (3) magma mixing.

Models of the major-element chemistry of the Sifton volcanics were performed using the thermodynamic algorithm MELTS of Ghiorso and Sack (1995), and were after verified by XSTALN, a computer program in which the fractionation of specific minerals is simulated using the solid solution expressions of Grove et al. (1982) for plagioclase, Beattie et al. (1991) for olivine and pyroxenes, and Nielsen and Dungan (1983) for spinels and ilmenite along with trace element K_d values from various sources (http://earthref.org/GERM/index.html?main.htm). The closed-system fractional crystallization models begin at the thermodynamically estimated liquidus temperature calculated by MELTS, and proceed until the residual melt reaches the high-SiO_2 rhyolitic composition. Due to the absence of true

basalts within the SRVC lavas, the most primitive and least altered basaltic andesite dyke (SF-136; 52.6 wt.% SiO_2; Mg # 79) was used as a model parental magma (Table 4). Clinopyroxene phenocrysts and subordinate plagioclase microlites constitute only 6 vol.% of this dyke, indicating that its composition approaches that of a liquid.

The SRVC major-element variations are best reproduced by MELTS models with relatively low water contents for a subduction-related magmatic suite (1.5–2.0 wt.% H_2O), pressures equivalent to upper crustal conditions (1.5 kbar), and fO_2 close to the QFM buffer (Fig. 12). Intensive and extensive parameters obtained from the MELTS program were subsequently used in a crystal fractionation model performed by the XSTALN algorithm, and the results were compared. Three fractionating intervals in the XSTALN model consist of crystalline assemblages identical to phenocryst phases observed in the SRVC lavas, with proportions optimized in order to reproduce the major-element chemistry. The limits of the fractionation steps were determined from inflections in major-element trends plotted on Harker-type diagrams against MgO content as a proxy for temperature.

1) Modeling the compositional range from basaltic andesite to dacite (52.0 to 61.0 wt.% SiO_2; 6.6 to 1.8 wt.% MgO) involved the extraction of plagioclase (20.0 wt.%), olivine (20.0 wt.%), clinopyroxene (40.0 wt.%), orthopyroxene (12.0 wt.%), ilmenite (6.0 wt.%), spinel (2.0 wt.%) and apatite (0.1 wt.%) over a temperature interval of 200 °C.

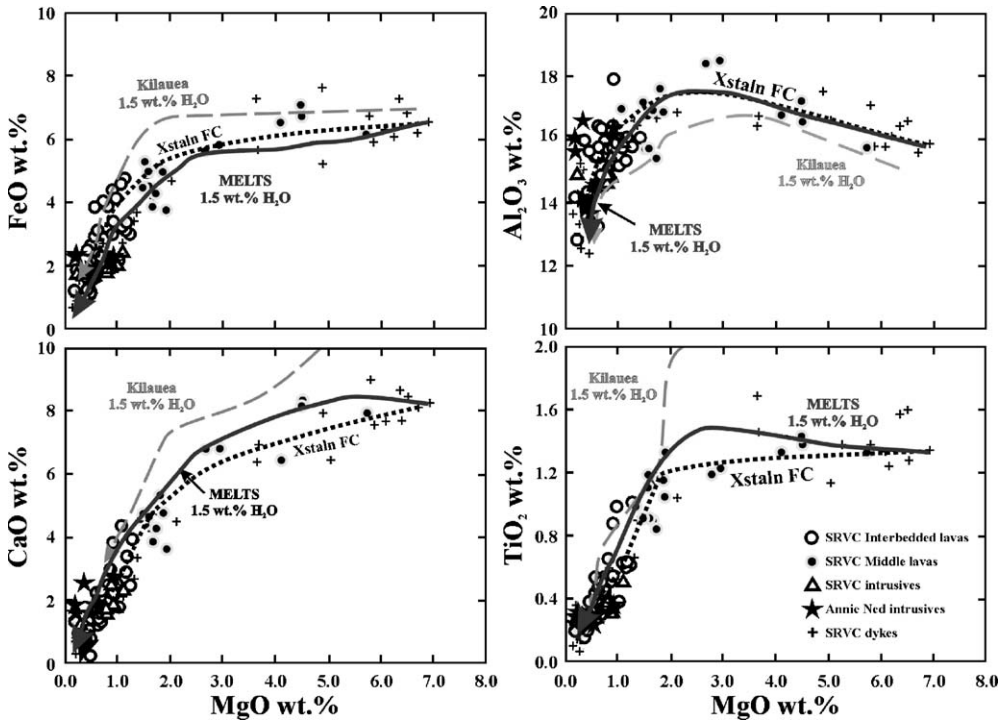

Fig. 12. Results of modeling the liquid line of descent for SRVC magmas with selected major elements. Runs were conducted at temperature intervals of 10 °C, and at oxygen fugacity conditions close to the QFM buffer. Pressure and water concentrations vary from anhydrous to 4 wt.% H_2O-saturated conditions and between 1 atm and 4 kbar, respectively. Arrows indicate compositional trends of residual liquids with progressive fractional crystallization plotted vs. MgO concentration as a proxy for temperature. Solid lines correspond to fractionation trends based on the MELTS thermodynamic algorithm of Ghiorso and Sack (1995); dashed lines are trends calculated by XSTALN. The modeled conditions correspond to 1.5 kbar pressure except for the 4 wt.% H_2O MELTS trend that was performed at 2.5 kbar. The compositional trend of residual glasses from 1.5 kbar, 1.5 wt.% H_2O melting experiments on a Kilauea tholeiitic basalt (Spulber and Rutherford, 1983) is shown for comparison.

Olivine remained in the fractionated assemblage until 5.0 wt.% MgO, at which point it disappears in the MELTS models, and is included only in a trace amount in XSTALN as a monitor for decreasing temperature.

2) The second step starts at 61 wt.% SiO_2, near the andesite–dacite transition, with a decrease in the abundance of clinopyroxene and a large increase in the proportion of plagioclase. Over the dacite compositional field (61.0 to 67.0 wt.% SiO_2; 1.8 to 0.9 wt.% MgO), the fractionation proportions are: plagioclase (37.0 wt.%), clinopyroxene (20.0 wt.%), orthopyroxene (25.0 wt.%), ilmenite (15.0 wt.%) and apatite (3.0 wt.%).
3) The final fractionation step begins at 67 wt.% SiO_2 and consists of orthoclase (40.0 wt.%), quartz (25.0 wt.%), albite (20.0 wt.%), magnetite (9.0 wt.%), and ilmenite (5.0 wt.%), as well as a trace of zircon. The sharp decrease in FeO observed in the SRVC rhyolites requires the fractionation of magnetite under redox values slightly above QFM buffer ($\Delta\log fO_2$ +0.5 to +1.0); conditions similar to those reported for the compositionally similar Bishop Tuff (Hildreth, 1977) and the Crater Lake rhyodacites (Druitt and Bacon, 1989).

The model proportions of fractionated crystals from XSTALN are generally in agreement with the fractionated assemblage from MELTS, as well as the modal proportions and abundances of phenocryst phases from the SRVC lavas (Table 2), with the exception of olivine which was not observed even in the most primitive SRVC basaltic andesites. The apparent population minimum within the Middle Lavas between 56 and 59 wt.% SiO_2 (Fig. 8A) is also evident in plots of Al_2O_3, FeO and CaO vs. MgO, and coincides with the modeled change in the relative proportions of minerals in the fractionating assemblage between the first and second fractionating steps.

The thermodynamic fractionation models predict the first plagioclase to be An_{75} in composition, which is comparable to the maximum anorthite content (An_{76}) observed in the basaltic andesite lavas, but is not as calcic as the rare bytownite crystals, and the rims (An_{80}) observed on some reversely zoned plagioclase phenocrysts in the evolved andesites (62 wt.% SiO_2) of the Middle Lavas (Fig. 6; Table 1). These higher anorthite contents probably reflect the presence of higher temperature magmas than the chosen parent. The variable An contents, presence of dissolution surfaces, reverse zoning, and sieve-like textures of plagioclase crystals within the lower Middle Lava flows also point to recharge of higher temperature magmas into a system undergoing differentiation. Reversely zoned clinopyroxenes in the two-pyroxene dacites of the lower Interbedded Unit, characterized by progressively increasing Mg # (42–70), and a decrease in the Ca/Na ratios (66–48), provide further evidence for mixing with relatively more primitive melts. Based on the calculation from the MELTS model at 1.5 kbar, and 1.5 wt.% H_2O, the observed range of the Mg # in the reversely zoned clinopyroxenes of the SRVC dacites would correspond to a decrease in the SiO_2 content of the host magma from 72 wt.% for the core to 56 wt.% for the rim, equivalent to an input of between 20 and 30 wt.% of a basaltic andesite melt into a rhyolitic magma chamber.

The SRVC rhyolites and granites cluster between the polybaric, H_2O-saturated cotectic in the Petrogeny's Residua system of Bowen (1935), and the 1.0 kbar, low-temperature valley of Carmichael and MacKenzie (1963). The systematic offset of the granite trend from the H_2O-saturated minimum melt compositions towards the $KAlSi_3O_8$ apex in the Qtz–Ab–Or system is consistent with a significant presence of Ca in the SRVC haplogranitic melt thus inducing a shift in the position of the Ab–Or cotectic (Ehlers, 1972; Fig. 9). Elevated Ca levels also account for the presence of two feldspars in the epizonal SRVC intrusives with rather high An contents of the granitic plagioclase (An_{50}). Furthermore, both the SRVC rhyolites and granites lie within the 1.0 kbar low-temperature trough, consistent with a shallow emplacement within the volcanic package, and suggest a temperature controlled evolution (i.e. feldspar fractionation) of the granitic melt where the intrusives and the rhyolitic lavas represent the higher and lower temperature melts, respectively. High anorthite contents found in the cyclically zoned plagioclase crystals of the SRVC granites (Table 1) are interpreted as reflecting inputs of higher temperature magmas into the fractionating, plagioclase-rich mush column. The fact that the SRCV felsic melts do not coincide with the minimum melt composition could imply a number of things; they could be in part cumulate, or simply liquids fractionating towards

the minimum melt composition. The position of the low temperature trough and minimum melt composition in the haplogranite system is further complicated by the presence volatiles other than water, primarily F and C (Johnson et al., 2003). The compositions of amphiboles from the Sifton Range granite indicate that the mole fraction of H_2O in the volatiles dissolved in the magma may have been as low as 0.43 (Table 1), thus further contributing to the offset of the plagioclase cotectic (Fig. 9). Collectively, these features are diagnostic of a more complex evolution for the SRVC granites relative to the SRVC rhyolites, and the possible role of crustal recycling in the granite petrogenesis involving open-system exchange between the residual haplogranitic liquid and partial (anatectic) melts occupying the upper part of the magma system. Although the Annie Ned granitoids lie closer to the H_2O-saturated ternary eutectic at 5 kbar, they point towards the 2 kbar minimum melt composition and are collinear with the 2 kbar cotectic, suggesting greater depths of crystallization relative to the SRVC intrusives. Translated into the height of the upper crustal rock column, the difference of 0.5–1 kbar is consistent with the structural (and topographic) offset between the Sifton granites and the Annie Ned pluton (i.e. 1.5–3 km).

Despite being able to reproduce the major element variation over the compositional range of the SRVC rocks, closed-system crystal fractionation models invariably fail to reproduce contents of the highly incompatible elements observed in the SRVC felsic lavas and the granites. This is particularly true for large ratios of LILE (Ba, Rb), Th and U relative to HFSE in the SRVC rhyolites and granites, but also for the degree of LREE fractionation (La/Sm), as well as HFSE ratios (Nb/Zr). Furthermore, the behavior of Pb, Th, and K appears to be a decoupled from Ce, La and Nb (Fig. 13), all of which are highly incompatible elements with similar partition coefficients during low-pressure crystallization (Pearce and Parkinson, 1993). This trace element behavior clearly indicates an open-system petrogenesis for the SRVC dacites, rhyolites and the granites requiring high degrees of crustal contamination.

Two methods were used in an attempt to reproduce the observed trends: (1) a simple binary mixing model between the parental basaltic andesite (SF-136) and a LILE and Th-enriched SRVC rhyolite (SF-77) from the Upper Interbedded Unit, and (2) an assimilation-fractional crystallization (AFC) process (DePaolo, 1981), in which the enriched rhyolitic melt is incrementally added to a fractionating basaltic andesite magma. Although the AFC model better predicts the variations in Th, Pb and REE relative to the binary mixing, which seems better correlated with the behavior of LILE and Nb, neither model fully accounts for the complete range of trace element concentrations in the SRVC. The discrepancy between the two models might reflect the higher diffusivity of LILE relative to HFSE during the mixing and contamination of silicate melts along steep chemical gradients (Pearce and Peate, 1995). This would eventually result in a selective contamination of primitive magmas by the wall-rocks as observed between picritic magmas and upper crust along margins of the Muskox layered intrusion in Nunavut Canada (Francis, 1994).

The energy-constrained assimilation-fractional crystallization (EC-AFC) scheme of Bohrson and Spera (2001) was used to quantify the extent and thermodynamic plausibility of upper crustal contamination, and the extent of assimilation was monitored through the increase in Th concentrations. Although typically grouped with the LIL elements (Pearce and Parkinson, 1993), the ionic potential of Th is intermediate between most LILE and HFSE, and it is less mobile than LILE during alteration (Pearce, 1983). Furthermore, the upper continental crust is particularly enriched in thorium relative to mantle-derived basaltic melts (Taylor and McLennan, 1995), thus making it an ideal index for quantifying the extent of upper crustal contamination ($Th_{(SRVC\ rhyolite)}/Th_{(parental\ magma)}=11$). The EC-AFC parameters (Table 4) were adjusted to replicate a scenario in which an initially aphyric mafic melt releases thermal energy during cooling until c.a. 6 vol.% crystallinity is attained, similar to the phenocryst content of the SRVC parental dyke, and is subsequently intruded into a hydrous (c.a. 2 wt.% H_2O) upper crust at a temperature equivalent to the measured geotherm at 5 km depth in the northern Canadian Cordillera (Lewis et al., 2003). The method assumes that the present, steady-state thermal regime places minimum-temperature constraints on the early Tertiary crustal conditions. The magmatic system is then allowed to thermally equilibrate and the extent of assimilation is monitored via the increase in Th. Because closed-system fractional

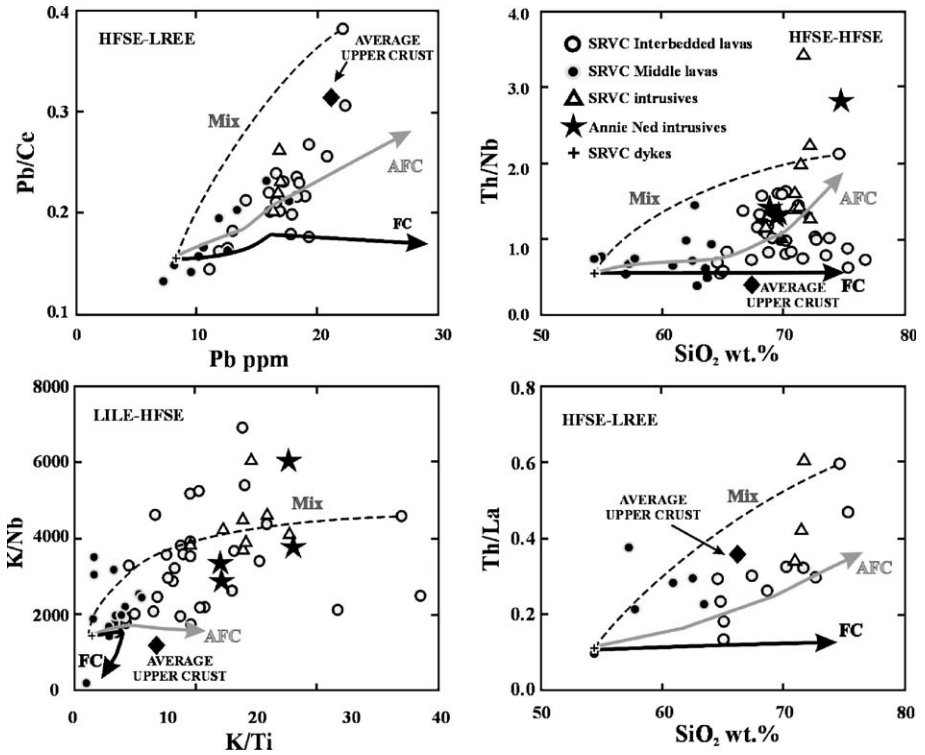

Fig. 13. SRVC trace element chemistry and the results of AFC and binary mixing models, respectively. All models involve the SRVC parental basaltic dyke (SF-136) and the high-silica SRVC rhyolite (SF-77) as either the assimilate or end-member composition during magma mixing. Fractional crystallization model at 1.5 kbar, and initial H_2O content of 1.5 wt.%; AFC—assimilation fractional crystallization (2nd step $r=0.95$; 3rd step $r>2.5$). Average upper crustal values after Taylor and McLennan (1995).

crystallization reproduces the Th contents observed in the andesites of the SRVC Middle Lavas, assimilation of enriched crust was restricted to the 2nd and 3rd fractionation steps (Fig. 14). Our AFC models require r factors, representing the ratio of assimilated to crystallized masses (DePaolo, 1981), of 0.57–0.95 during the 2nd fractionation step, and $r>2.5$ ratios during the 3rd stage of fractionation. The mass of assimilant required to replicate Th content of the rhyolites and granites in the last fractionating step thus exceeds the original magma mass by more than 150 wt.%.

The effectiveness of any assimilation process is essentially constrained by the thermal budget of the assimilating magma and the fertility of the wall rock contaminant (Marsh, 1989). For example, pelitic lithologies with relatively low solidus temperatures are more readily assimilated by mafic magmas than tonalites (Thompson et al., 2002). Likewise, the higher liquidus temperatures of picritic basalts (1350 °C) make them more capable of assimilating crust than basaltic andesites at approximately 1050 °C. The long-held view that the assimilated mass cannot surpass the amount of crystallized cumulate because of thermal constraints has been challenged by thermodynamic studies of Reiners et al. (1995), which suggest the possibility of r factors substantially greater than one (2.0–3.0). However, such large factors are restricted to basaltic magmas during a narrow isenthalpic AFC interval, and only when intruded into preheated upper crustal lithologies. Following the appearance of plagioclase and clinopyroxene on liquidus, the assimilation factors tend to decrease to less than one.

The very large r factors required in the 3rd fractionating stage of our AFC models, and the increase in the assimilated mass with progressive crystallization contradict the behavior expected for a cooling mag-

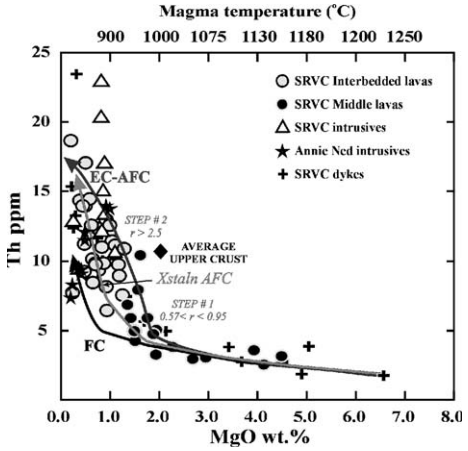

Fig. 14. Th vs. MgO plot summarizing AFC (XSTALN) and energy-constrained AFC models of crustal assimilation during petrogenesis of the Sifton Range magmas. FC-fractional crystallization (1.5 kbar, 1.5 wt.% H_2O); AFC—assimilation fractional crystallization (2nd step $r=0.95$; 3rd step $r>2.5$); EC-AFC—energy-constrained assimilation-fractional crystallization of Bohrson and Spera, 2001 (2nd step $r=0.57$; 3rd step $r>6$). Magma temperature estimates from the MELTS and XSTALN models; details of the AFC and EC-AFC modeling are outlined in Table 4.

matic system. This suggests that the incompatible element enriched SRVC rhyolites and granites may have been produced by crustal anatexis, rather than by small-scale contamination of mantle-derived magmas. Comparison of the SRVC magma composition with experimentally derived melts of Gerdes et al. (2000) provides some support for this proposal. In a diagram of $Al_2O_3/(MgO+FeO^*)$ vs. $CaO/(MgO+FeO^*)$, the majority of the SRVC rhyolites, dacites and granites fall within the field defined by partial melting of metasedimentary sources (greywackes and pelites) and are clearly distinct from the (basaltic) andesites that occupy metabasalt and metatonalite protoliths (Fig. 15). These observations are indicative of the coexistence of two different magma types in the SRVC system, one mantle-derived that evolved to the basaltic andesites of the Middle Lavas, and another crust-derived which gave rise to the rhyolites and corresponding intrusives. Moderate to high assimilation factors (0.57–0.95) required in the AFC models between 61 and 67 wt.% SiO_2 are equivalent to up to 33 wt.% of rhyolite contamination and suggest that the SRVC dacitic magmas may in fact be hybrids between mantle and crustal melts.

The northern Canadian Cordillera in the Sifton area is characterized by high heat flow (4.8 uW/m^3), relatively low crustal thicknesses (30–32 km; Flück et al., 2003), and is underlain by a zone of anomalously hot mantle (Shi et al., 1998). Lewis et al. (2003) have estimated relatively high temperatures of 800–900 °C at the Moho throughout the Canadian Cordillera, with a slight increase in heat flux north of the 59° N latitude. They suggest that the present thermal regime across the Cordillera reflects the past several 100 Ma, possibly extending to the initiation of east-dipping subduction below the western margin of North American craton in the Middle Devonian. Despite a diversity of opinions on the composition of crust below the northern Canadian Cordillera (Hammer et al., 2000), geological mapping and geochemical characterization has revealed relatively fertile lithologies below the northernmost CPC extending to mid-crustal levels (Hart, 1995, 1997). The ascent of mantle-derived melts into such fertile middle to upper crustal regions could result in large-scale crustal anatexis, and in some cases, associated felsic magmatism. Based on the work in the Sloko Lake volcanic complex which represents the largest Paleocene volcanic suite of the northern Canadian Cordillera, Resnick (2003) recognized two major rhyolitic units, one of which straddles the 0.5 kbar eutectic minimum on the Qtz–Ab–Or–H_2O pseudo-ternary diagram and was interpreted as the product of

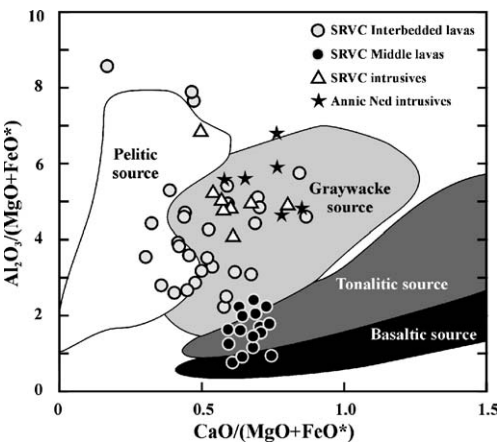

Fig. 15. $Al_2O_3/(FeO^*+MgO)$ vs. $CaO/(FeO^*+MgO)$ for the Sifton Range volcanic complex. Outlined fields indicate compositions of experimentally determined partial melts from a variety of protoliths under H_2O-saturated conditions (Gerdes et al., 2000).

crustal anatexis (Fig 9). If crustal melting is indeed responsible for the genesis of some of the early Tertiary felsic lavas and granites in the northern Canadian Cordillera, however, the near chondritic isotopic signatures of the Eocene Nisling Plutonic Suite ($0.7045 < {}^{87}Sr/{}^{86}Sr_i < 0.705$; Hart, 1995), as well as the SRVC-coeval Bennett Lake and Mt. Skukum volcanics ($0.70495 < {}^{87}Sr/{}^{86}Sr_i < 0.70530$ and $\epsilon_{Nd} = +0.8$ to -0.5; Morris and Creaser, 2003), suggests that the crustal components involved were both young and isotopically juvenile at the time of partial melting. In case of the SRVC, this excludes any possibility of large-scale anatexis of the local Precambrian Nisling Schist basement, which by late Mesozoic time would have exceeded ${}^{87}Sr/{}^{86}Sr_i$ of 0.710 (Morrison et al., 1979). The decoupling of LILE and HFSE observed in the early Tertiary magmas further points to the likely subduction-related signature of the felsic source. One of the ways to satisfy these geochemical criteria (i.e. felsic compositions, primitive isotopic ratios and high LILE/HFSE) is to contribute significant quantities of rapidly buried, young, island arc material. The suitable candidates within the upper crust of the southwestern Yukon include dacitic to trachytic volcanics and hypabyssal intrusives of the early Jurassic Hazelton volcanics (Wheeler and McFeely, 1991), as well as granodiorites of the early Jurassic Aishihik Lake suite and other late Mesozoic CPC intrusive suites (Templeman-Kluit and Currie, 1978).

5.3. SRVC magma rheology and eruptibility

The Sifton Range volcanic stratigraphy records an intimate relationship between eruption style and chemical composition. The explosive volcanic activity responsible for the felsic agglomerates and lapilli tuffs of the Lower Interbedded Unit changed to the effusive outpourings of the more mafic basaltic andesites of the Middle Lavas, and then, once again, shifted to the explosive activity of the felsic Upper Interbedded Unit. There is a gradual decrease in the abundance of dacite and rhyolite lavas above 62 wt.% SiO_2 which are gradually replaced by the explosive eruption of magmas with more than 68 wt.% SiO_2, the latter corresponding to the compositional range of the coeval granitoid pluton (Fig. 7). Quantitative rheological modeling of an evolving silicate melt was undertaken to investigate these correlations. Bottinga and Weill (1972), Kushiro (1980) and Pinkerton and Norton (1995) have shown that the viscosity of crystal-free silicate melts will increase with increasing polymerization (i.e. SiO_2 wt.%), lowered volatile content and a reduction in total pressure. Water content is particularly important because H_2O molecule dissociates in silicate melts to H^+ and OH^- ions which disrupt Si–O–Si bonds and depolymerize the melt (Burnham, 1979). Recent studies (Lejeune and Richet, 1995) have shown that the influence of the suspended phenocrysts on the viscosity of magmas becomes critically important above 40 vol.%, at which point a distinct non-Newtonian behavior is observed (Marsh, 1981).

The viscosities of fractionating SRVC magmas were calculated for modeled rock compositions at different pressures and H_2O concentrations, following the procedure of Shaw (1972). These calculations take into account the competing effects of temperature, pressure, SiO_2 and H_2O content on the viscosity of melts (McBirney and Murase, 1984). The commonly used Einstein–Roscoe equation (Roscoe, 1953):

$$\mu = \mu_0(1 - \Phi/\Phi_m)^{-2.5}$$

in which μ is the effective viscosity of a liquid containing a volume Φ of suspended solids, and where maximum packing efficiency (Φ_m) is 0.6 (Pinkerton and Stevenson, 1992)? was subsequently incorporated to account for the effects of crystallinity, which exceeds 30 vol.% in the evolved SRVC andesites. The solid assemblages predicted at each increment of fractional crystallization were added back into the melt and cumulative viscosities were calculated for the crystalline suspensions. The results of rheological modeling illustrate the profound dependence of viscosity on crystal content (Fig. 16). Calculations of the effective magma viscosity carried out with XSTALN and MELTS on compositions at conditions that best fit the SRVC major-element chemistry (1.5 kbar, 1.5 wt.% H_2O), indicate a rapid increase in viscosity from 10^6 to 10^{10} Pa s near the beginning of 2nd fractionation step (62 wt.% SiO_2), following a 17 wt.% increase in the proportion of crystallizing feldspar. The calculated crystal contents in our models generally agree with the observed SRVC phenocryst proportions, especially during the early stages of magma differentiation (Table 2). Plagioclase is the dominant phenocryst in the SRVC, and as shown by Philpotts et al. (1998) and Saar et al.

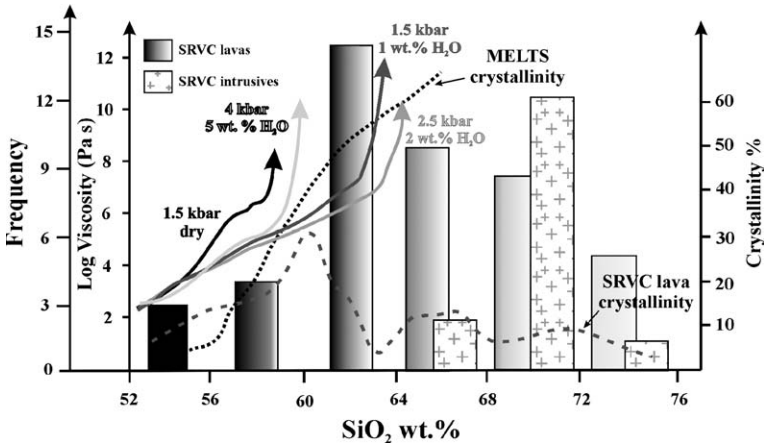

Fig. 16. Results of magma rheology modeling in the context of compositional distribution of the SRVC volcanic and plutonic rocks on a SiO_2 histogram. Computed viscosities are based on residual liquid compositions from MELTS and XSTALN, whereby fractionated solid assemblages at each increment are added back into the melt, and assume critical crystallinity corresponding to the second rheological threshold (c.a. 60–74 vol.%; Wickham, 1987).

(2001), the large aspect ratios of plagioclase crystals (up to 1:4:16) enable them to form continuous 3D frameworks capable of providing yield strength in basaltic magmas at crystallinities as low as 8–21 vol.%. It is therefore expected that the plagioclase contents in excess of 30 vol.% found in the evolved SRVC andesites might generate shear strengths that would significantly impede magma flow, causing a progressive reduction in the likelihood of the effusive eruption of more felsic lavas. We interpret an apparent paradox whereby the most frequently erupted rock type is also the one characterized by the highest crystallinity as an artifact of the overall low abundances of the SRVC (basaltic) andesite lavas. The importance of magma crystallinity during the eruption of the SRVC lavas herein lies in a coincidence between the achievement of maximum values and a sudden reversal in the trend of continuously increasing volumes of erupted magma with increasing SiO_2 contents.

The differences between viscosity trends are primarily due to the effects of water concentration on the point of appearance of plagioclase on the liquidus, and its relative proportions in the crystallizing assemblage, which in turn seems to be the dominant control on the effective magma viscosities. Higher water concentrations tend to reduce the stability field of plagioclase relative to those of olivine and clinopyroxene, thus delaying appearance of plagioclase on the liquidus (Baker and Eggler, 1987). Consequently, hydrous magmas will not achieve critical viscosities until higher SiO_2 contents due to both the depolymerizing effect of water on the melt and the delay of the appearance of plagioclase as a crystallizing phase. Once plagioclase appears at elevated water pressures, however, its proportion relative to clinopyroxene and olivine in the crystallizing assemblage is much higher (Gaetani et al., 1993). This can lead to a scenario in which magma becomes supersaturated in plagioclase upon water loss, and resultant crystallization in turn quickly overwhelms the system causing a rapid increase in viscosity as shown by the 4.5 wt.% H_2O viscosity trend (Fig. 16).

5.4. Petrogenesis by interaction of two magmas

The juxtaposition of the closed-system fractionated andesites of the SRVC Middle Lavas with the dominantly anatectic rhyolites of the Interbedded Units, the presence of andesitic blocks in rhyolitic matrices of the SRVC fragmental volcanics, as well as the reversely zoned clinopyroxenes of the hybrid SRVC dacites all suggest the coexistence and interaction between two magmas of different origin. The sieved–textured bytownite crystals in disequilibrium with their andesitic matrix also indicate that the

SRVC magmatic system was subject to rejuvenation by mantle-derived magmas during the course of its evolution. Sparks et al. (1977) and Bachmann et al. (2002) have proposed that both felsic pyroclastic volcanism and granite plutonism can be generated during ascent and replenishment of a shallow felsic crustal chamber by hotter, mafic magmas. The commonly held view is that the thermally-induced convection and rapid magma overturn lead to water saturation and eventual degassing that ultimately results in both explosive eruptions and the rapid crystallization of the remaining magma to form shallow granite plutons (Eichelberger and Westrich, 1981).

The point of water saturation along the liquid line of decent is closely related to the onset of the explosive volcanism in the SRVC, and may have been a critical factor in the eruption of the pyroclastic rocks. Volatile exsolution and over-pressurization of shallow magma chambers is currently the preferred mechanism for the genesis of silicic pyroclastics (Gerlach et al., 1994; Sparks, 1997; Bower and Woods, 1998). Once the solubility limit of volatiles is reached in the shallow reservoirs, magma is quickly converted to a highly vesicular (bubbly) liquid, which ascends and ponds beneath the chamber roof (Sparks, 1978). Our 1.5 kbar fractionation models with initial H_2O concentrations of 1.5 wt.% reach saturation within the dacite field at c.a. 65 wt.% SiO_2, and agree with the experimentally determined solubility of water in dacite and rhyolite glasses (Pineau et al., 1998; Holtz et al., 2000; Moore et al., 1998). Numerous recent studies (Stein and Spera, 1992; Dingwell, 1996; Manga et al., 1998; Massol and Jaupart, 1999) have also shown that under low shear stresses, the viscosity of a magma containing vapour bubbles increases with the bubble volume fraction, which in turn facilitates fragmentation and eruption of pyroclastics. Both lines of evidence are consistent with a model in which the exsolution and ascent of water from the evolved SRVC dacites undergoing AFC crystallization in a compositionally stratified magma chamber was responsible for explosive eruptions of the overlying rhyolitic melt when the hydrostatic pressure exceeded the lithostatic pressure. Sudden loss of volatiles from the upper rhyolite layer upon eruption would induce late-stage plagioclase crystallization in the remaining part of the chamber by elevating the temperature of the An–Ab solidus–liquidus loop (Wyllie, 1963). The associated further increase in viscosity could be the crucial factor in the final solidification of rhyolitic crystal mush to form the SRVC plutonic rocks.

We propose that the episodic injection of a higher temperature, mafic melt into the shallow SRVC magma system was the reason for initiating the volcanic activity, and in turn promoted SRVC plutonism. The intrusion of mantle-derived basaltic melts into the upper granodioritic crust of the Coast Plutonic Complex (CPC) induced localized anatexis, and the formation of a stratified magma reservoir in which an upper layer of crustally-derived rhyolite was separated from underlying andesite magma by a hybrid dacite. In this model, the relatively high viscosity of the evolved andesites impeded mixing with the anatectic rhyolite and precluded the wholesale chamber homogenization. Interaction between the two magmas within the contact zone of such a compositionally stratified magmatic system would produce the intervening layer of hybrid dacites. The evidence supporting magma mixing is widespread in the pyroclastic breccias and lapilli tuffs of the Lower Interbedded Unit, where compositionally contrasting basaltic andesite blocks and lapilli fragments tend to be incorporated in rhyolitic matrices. Subsequent episodes of mafic replenishment and magma mixing were associated with release of volatiles from the hybrid dacites, as well as the fractionating mafic magmas. Exsolved water bubbles permeated the overlying anatectic magma, and the resultant overpressure lead to the explosive eruption of the rhyolitic pyroclastic rocks. Episodes of explosivity were terminated by the eruption of degassed rhyolite flows, followed by hybrid dacitic flows from the deeper parts of the SRVC magma chamber. Repetition of this process would account for the alternating beds of pyroclastic ejecta with rhyolite and dacite flows within the SRVC Interbedded Units. The presence of andesites in the Middle Lavas suggests that the felsic anatectic and hybrid magmas were eventually completely flushed from the reservoir, consistent with models of Marti et al. (2000) and Bower and Woods (1998), which suggest that once initiated, caldera-forming eruptions associated with siliceous pyroclastic ejecta tend to empty most of the magma from the shallow, volatile-rich chamber. Following the loss of volatiles asso-

ciated with extensive explosive eruptions of the upper pyroclastics, any interstitial rhyolitic liquid left in the crystalline mush would rapidly crystallized feldspar that accumulated and facilitated the formation of the SRVC granite.

6. Conclusions

The petrogenesis of the Sifton Range volcanic complex in the southern Yukon was dominated by the interaction between basaltic andesite magmas originating from a mantle source at less than 65 km depth, and highly enriched rhyolitic magmas derived by melting of the upper crust of the northern Coast Plutonic Complex. The SRVC andesites evolved via low-pressure, closed-system crystal fractionation from mantle-derived parents under damp conditions, whereas the dacites represent hybridized magmas produced by interaction with the crustally-derived rhyolite magma. The enrichment in highly incompatible trace elements displayed by the SRVC granites and rhyolites suggests that they were derived by anatexis of an upper crustal meta-greywacke to meta-pelitic protolith. The relatively low initial Sr and Nd isotope ratios of the coeval volcanic and plutonic rocks in the northern Canadian Cordillera, however, require anatexis of isotopically juvenile crust. The mafic lavas are stratigraphically bracketed by rhyolite flows and pyroclastics containing andesitic fragments and suggest the coexistence of these two magmas in a zoned magma chamber with crustally-derived rhyolite separated from underlying mantle-derived andesite by a zone of hybrid dacites. The prominent population mode of the SRVC lavas near the andesite–dacite transition, and the transition from effusive mafic to explosive rhyolitic volcanism are probably related to the effect of water on the rheological behavior of the magmatic system. Critical plagioclase crystallinities did not occur until the mantle-derived magma reached dacitic compositions via crystal fractionation, at which point it became too viscous to erupt effusively. The explosive volcanism in the SRVC may have resulted from water exsolution in the hybrid dacitic magma induced by the recharge of juvenile mafic melt. Finally, the granitic intrusives may reflect the rapid increase in plagioclase content in the degassed crustal melt leading to magma stagnation and plutonism.

Acknowledgements

The authors thank Craig Hart of the Yukon Geological Survey for logistical support and field expertise. The first author is greatly indebted to the staff of the McGill University Geochemical Laboratories for conducting the analytical work. U/Pb dating of the Sifton Range granite was conducted by Jim Mortensen at the Pacific Centre for Isotopic and Geochemical Research (PCIGR) at the University of British Columbia in Vancouver. Critical reviews of Dante Canil, James Scoates, Benjamin Edwards and Kelly Russell greatly improved the quality of text. This work was supported by the NSERC Discovery grant (Francis) and Northern Scientific Training Program grants (Francis, Mišković).

References

Aitken, J.D., 1959. Atlin map-area, British Columbia, Geological Survey of Canada, Memoir 307. 89 p.

Arakawa, Y., Shinmura, T., 1995. Nd–Sr isotopic and geochemical characteristics of two contrasting types of calc-alkaline plutons in the Hida Belt, Japan. Chemical Geology 124, 217–232.

Bachmann, O., Dungan, M.A., Lipman, P.W., 2002. The Fish Canyon magma body, San Juan Volcanic Field, Colorado: rejuvenation and eruption of an upper-crustal batholith. Journal of Petrology 43, 1469–1503.

Bailey, E.H., Ragnasdottir, K.V., 1994. Uranium and thorium solubilities in subduction zone fluids. Earth and Planetary Science Letters 124, 119–129.

Baker, D.R., Eggler, D.H., 1987. Composition of melts coexisting with plagioclase, augite and olivine or low-calcium pyroxene at pressures from one atmosphere to 8 kbar, anhydrous and 2 percent H_2O and applications to island arc petrogenesis. American Mineralogist 72, 12–28.

Barker, F., Arth, J.G., Stern, T.W., 1986. Evolution of the coast batholith along the Skagway Traverse, Alaska and British Columbia. American Mineralogist 71, 632–643.

Bateman, P.C., Eaton, J.P., 1967. Sierra Nevada Batholith, California. Science 158 (3807), 1407–1417.

Bateman, P.C., Clark, L.D., Huber, N.K., Moore, J.G., Reinhart, C.D., 1963. The Sierra Nevada Batholith—a synthesis of recent work across the central part. U.S. Geological Survey Professional Paper 414D, D1–D46.

Beattie, P., Ford, C., Russell, D., 1991. Partition coefficients for olivine-melt and orthopyroxene-melt systems. Contributions to Mineralogy and Petrology 109, 212–224.

Berman, R.G., 1981. Differentiation of calc-alkaline magmas; evidence from the Coquihalla volcanic complex, British Columbia. Journal of Volcanology and Geothermal Research 9, 151–179.

Bohrson, W., Spera, F.J., 2001. Energy-constrained open-system magmatic processes: II. Application of energy-constrained assimilation-fractional crystallization (EC-AFC) model to magmatic systems. Journal of Petrology 42 (5), 1019–1041.

Brophy, J.G., 1991. Composition gaps, critical crystallinity, and fractional crystallization in orogenic magmatic systems. Contributions to Mineralogy and Petrology 109, 173–182.

Bottinga, Y., Weill, D.F., 1972. The viscosity of magmatic silicate liquids: a model for calculation. American Journal of Sciences 272, 438–475.

Bowen, N.L., 1935. The igneous rocks in light of high temperature research. Scientific Monitor 40, 403–487.

Bower, S.M., Woods, A.W., 1998. On the influence of magma chambers in controlling the evolution of explosive volcanic eruptions. Journal of Volcanology and Geothermal Research 86, 67–78.

Brandon, A.D., Draper, D.S., 1998. Reply to comment by B.R. Frost and C. Ballhouse on "Constraints on the origin of the oxidation states of mantle overlying subduction zones: an example from Simcoe, Washington, USA". Geochimica et Cosmochimica Acta 62, 333–335.

Burnham, C.W., 1979. The importance of volatile constituents. In: Yoder, H.S. (Ed.), The Evolution of the Igneous Rocks. Princeton University Press, New Jersey, pp. 439–482.

Carmichael, I.S.E., MacKenzie, W.S., 1963. Feldspar–liquid equilibria in pantellerites: an experimental study. American Journal of Science 261, 382–396.

Clague, D.A., Dalrymple, G.B., 1987. The Hawaiian–Emperor volcanic chain: Part I. Geologic evolution. In: Decker, R.W., Wright, T.L., Stauffer, P.H. (Eds.), Volcanism in Hawaii, U.S. Geological Survey Professional Paper, pp. 5–73.

DePaolo, D., 1981. Trace element and isotopic effects of combined wallrock assimilation and fractional crystallization. Earth and Planetary Science Letters 53, 189–202.

Dingwell, D.B., 1996. Volcanic dilemma: flow or blow? Science 273, 1054–1055.

Droop, G.T.R., 1987. A general equation for estimating Fe^{3+} concentrations in ferromagnesian silicates and oxides from microprobe analyses, using stoichiometric criteria. Mineralogical Magazine 51, 431–435.

Druitt, T.H., Bacon, C.R., 1989. Petrology of the zoned calc-alkaline magma chamber of Mount Mazama, Crater Lake, Oregon. Contributions to Mineralogy and Petrology 101, 245–259.

Ehlers, E.G., 1972. The Interpretation of Geological Phase Diagrams. W.H. Freeman and Co., San Francisco. 280 pp.

Eichelberger, J.C., 1995. Silicic volcanism: ascent of viscous magmas from crustal reservoirs. Annual Review of Earth and Planetary Sciences 23, 41–63.

Eichelberger, J.C., Westrich, J.C., 1981. Magmatic volatiles in explosive rhyolitic eruptions. Geophysical Research Letters 8, 757–760.

Engebretson, D.C., Cox, A., Gordon, R.G., 1985. Relative Motions Between Oceanic and Continental Plates in the Pacific Basin, Special Paper, vol. 206. Geological Society of America. 59 pp.

Flück, P., Hyndman, R.D., Lowe, C., 2003. Effective elastic thickness Te of the lithosphere in western Canada. Journal of Geophysical Research 108 (B9), 2430. doi:10.1029/2002JB002201.

Francis, D., 1994. Chemical interaction between picritic magmas and upper crust along margins of the Muskox Intrusion, Northwest Territories. Geological Survey of Canada Paper, vol. 92-12. 94 pp.

Francis, D., 2002. Interrogating the lithosphere of the northern Canadian Cordillera with Cretaceous to recent volcanics and mantle xenoliths. In: Cook, F., Hammer, P.T.C., Clowes, R.M. (Eds.), Slave-Northern Cordillera Lithospheric Evolution (SNORCLE) Workshop Meeting, Sidney, B.C., Lithoprobe Report, vol. 82.

Frost, B.R., Lindsley, D.H., 1992. Equilibria among Fe–Ti oxides, pyroxenes, olivine and quartz: Part II. Application. American Mineralogist 77, 1004–1020.

Fuhrman, M.L., Lindsley, D.H., 1988. Ternary-feldspar modeling and thermometry. American Mineralogist 73, 201–215.

Gabrielse, E.H., Yorath, C.J., 1991. Introduction, Chapter 1. In: Gabrielse, E.H., Yorath, C.J. (Eds.), Geology of the Cordilleran Orogen in Canada, Geology of Canada, vol. G-2. Geological Survey of Canada, pp. 5–11.

Gabrielse, E.H., Monger, J.W.H., Wheeler, J.O., Yorath, C.J., 1991. Part A. Morphogeological belts, tectonic assemblages, and terranes. In: Gabrielse, E.H., Yorath, C.J. (Eds.), Geology of the Cordilleran Orogen in Canada, Geology of Canada, vol. G-2. Geological Survey of Canada, pp. 15–28. E.H.

Gaetani, G.A., Grove, T.L., Bryan, W.B., 1993. The influence of water on the petrogenesis of subduction-related igneous rocks. Nature 365, 332–334.

Gerdes, A., Worner, G., Henk, A., 2000. Post-collisional granite generation and HAT-Lp metamorphism by radiogenic heating: the example from the Variscan South Bohemian Batholith. Journal of the Geological Society London 157, 577–587.

Gerlach, T.M., Westrich, H.R., Casadevall, T.J., Finnegan, D.L., 1994. Gas-saturated magma and SO_2, Cl, CO_2 emissions, 1989–1990 eruption, Redoubt Volcano, Alaska—an analysis of volatile emission estimates by melt inclusion, remote sensing and plume sampling techniques. Journal of Volcanology and Geothermal Research 62, 317–338.

Ghiorso, M.S., Sack, R.O., 1995. Chemical mass transfer in magmatic processes: IV. A revised and internally consistent thermodynamic model for the interpolation and extrapolation of liquid–solid equilibria in magmatic systems at elevated temperatures and pressures. Contributions to Mineralogy and Petrology 119, 197–212.

Gill, J.B., 1981. Orogenic Andesites and Plate Tectonics. Springer-Varlag, New York. 390 pp.

Gordey, S.P., Makepeace, A.J., 1999. Yukon digital geology. Geological Survey of Canada Open File D3826 and Exploration and Geological Services Division, Yukon, Indian and Northern Affairs Canada, Open File 1999-1(D).

Govindaraju, K., 1994. Compilation of working values and descriptions for 383 geostandards. Geostandards Newsletter 18, 1–158.

Green, T.H., 1972. Crystallization of calc-alkaline andesite under controlled high-pressure hydrous conditions. Contributions to Mineralogy and Petrology 34, 150–166.

Grove, T.L., Gerlach, D.C., Sando, T.W., 1982. Origin of calc-alkaline series lavas at Medicine Lake volcano by fractionation, assimilation and mixing. Contributions to Mineralogy and Petrology 80, 160–182.

Grove, T.L., Donnelly-Nolan, J.M., Housh, T., 1997. Magmatic processes that generated the rhyolite of Glass Mountain, Medicine Lake Volcano, N California. Contributions to Mineralogy and Petrology 127, 205–223.

Grove, T.L., Elkins-Tanton, L.T., Parman, S., W.,, Chatterjee, N., Muentener, O., Gaetani, G.A., 2003. Fractional crystallization and mantle-melting controls on calc-alkaline differentiation trends. Contributions to Mineralogy and Petrology 145, 515–533.

Hammer, P.C.T., Clowes, R.M., Ellis, R.M., 2000. Crustal structure of NW British Columbia and SE Alaska from seismic wide-angle studies: Coast Plutonic Complex to Stikinia. Journal of Geophysical Research 105, 7961–7981.

Hart, C.J.R, 1995. Magmatic and tectonic evolution of the Intermontane Superterrane and Coast Plutonic Complex in the southern Yukon Territory. M.Sc. Thesis, The University of British Columbia. 198 p.

Hart, C.J.R, 1997. A transect across northern Stikinia: geology of the Northern Whitehorse map area, southern Yukon Territory (105D/13-16). Exploration and Geological Services Division, Yukon Region, Indian and Northern Affairs Canada, Bulletin, vol. 8. 112 pp.

Hasik, V., 1994. Volcanic evidence for a compositional contrast in the lithospheric mantle across the Tintina Trench, southeastern Yukon. M.Sc. Thesis, McGill University, Montréal, Québec, Canada.

Hildreth, W., 1977. The magma chamber of the Bishop Tuff: gradients in temperature, pressure and composition. PhD Thesis. University of California, Berkley, California, The United States of America.

Hildreth, W., Moorbath, S., 1988. Crustal contributions to arc magmatism in the Andes of Central Chile. Contributions to Mineralogy and Petrology 98, 455–489.

Hollister, L.S., 1982. Metamorphic evidence for rapid (2 mm/yr) uplift of a portion of the Central Gneiss Complex, Coast Mountains, British Columbia. Canadian Mineralogist 20, 319–332.

Holtz, F., Roux, J., Behrens, H., Pichavant, M., 2000. Water solubility in silica and quartzofeldspathic melts. American Mineralogist 85, 682–686.

Jenner, G.A., Longerich, H.P., Jackson, S.E., Fryer, B.J., 1990. ICP-MS—a powerful tool for high precision trace element analysis in earth sciences: evidence from analysis of selected USGS reference samples. Chemical Geology 83, 133–148.

Johnson, T.E., Hudson, N.F.C., Droop, G.T.R., 2003. Evidence for genetic granite–migmatite link in the Dalradian of NE Scotland. Journal of the Geological Society (London) 160, 447–457.

Kawamoto, T., 1996. Experimental constraints on differentiation and H_2O abundance of calc-alkaline magmas. Earth and Planetary Science Letters 144, 577–589.

Kindle, E.D., 1953. Dezadeash map-area, Yukon Territory (1019A, 1: 253 440 scale). Geological Survey of Canada, Memoir 268, 58 p.

Kushiro, I., 1980. Viscosity, density and structure of silicate melts at high pressures, and their petrological applications. In: Hargraves, R.B. (Ed.), Physics of Magmatic Processes Princeton, New Jersey. Princeton University Press, pp. 93–120.

Lambert, M.B., 1974. The Bennett Lake cauldron subsidence complex, British Columbia and Yukon Territory. Geological Survey of Canada Bulletin 227 (213 pp.).

Lejeune, A., Richet, P., 1995. Rheology of crystal bearing melts: an experimental study at high viscosities. Journal of Geophysical Research 100 (B3), 4215–4229.

Lewis, T.J, Hyndman, R.D., Flück, P., 2003. Heat flow, heat generation, and crustal temperatures in the northern Canadian Cordillera: thermal control of tectonics. Journal of Geophysical Research 108 (B6), 2316. doi:10.1029/2002JB002090.

Le Maitre, R.W., 1989. A Classification of Igneous Rocks and Glossary of Terms. Blackwell Scientific Publications. 193 pp.

Manga, M., Castro, J., Cashman, K.V., Loewenberg, M., 1998. Rheology of bubble-bearing magmas: theoretical results. Journal of Volcanology and Geothermal Research 87, 3011–3013.

Marsh, B., 1981. On the crystallinity, probability of occurrence, and rheology of lava and magma. Contributions to Mineralogy and Petrology 78, 85–98.

Marsh, J., 1989. Geochemical constraints on coupled assimilation and fractional crystallization involving upper crustal compositions and continental tholeiitic magma. Earth and Planetary Science Letters 92, 70–80.

Marti, J., Folch, A., Neri, A., Macedonio, G., 2000. Pressure evolution during explosive caldera-forming eruptions. Earth and Planetary Science Letters 175, 275–287.

Massol, H., Jaupart, C., 1999. The generation of gas overpressure in volcanic eruptions. Earth and Planetary Science Letters 166, 57–70.

McBirney, A.R., Murase, T., 1984. Rheological properties of magmas. Annual Reviews of Earth and Planetary Sciences 12, 337–357.

McDonough, W.F., Sun, S.S., 1995. Composition of the Earth. Chemical Geology 120, 223–253.

Monger, J.W., Price, R., 2002. The Canadian Cordillera: geology and tectonic evolution. Canadian Society of Exploration Geophysicists Recorder, February 2002 ed., pp. 17–36.

Moore, G., Vennemann, T., Carmichael, I.S.E., 1998. An empirical model for the solubility of H_2O in magmas to 3 kilobars. American Mineralogist 83, 36–42.

Morris, R., Creaser, R., 2003. Crustal recycling during subduction at the Eocene Cordilleran margin of North America: a petrogenetic study from the southwestern Yukon. Canadian Journal of Earth Sciences 40, 1805–1821.

Morrison, G.W., Godwin, C.I., Armstrong, R.L., 1979. Interpretation of isotopic ages and $^{87}Sr/^{86}Sr$ initial ratios for plutonic rocks in the Whitehorse map area, Yukon. Canadian Journal of Earth Sciences 16, 1988–1997.

Miyashiro, A., 1974. Volcanic rock series in island arcs and active continental margins. American Journal of Science 274, 321–355.

Nielsen, R.L., Dungan, M.A., 1983. Low pressure mineral-melt equilibria in natural anhydrous mafic systems. Contributions to Mineralogy and Petrology 84, 310–326.

Peccerillo, A., Wu, T.W., 1992. Evolution of calc-alkaline magmas in continental arc volcanoes; evidence from Alicudi, Aeolian Arc (southern Tyrrhenian Sea, Italy). Journal of Petrology 33, 1295–1315.

Pearce, J.A., 1983. Role of the sub-continental lithosphere in magma genesis at active continental margins. In: Hawkesworth, C.J., Norry, M.J. (Eds.), Continental Basalts and Mantle Xenoliths, pp. 230–249.

Pearce, J.A., Parkinson, I., J.,, 1993. Trace-element models for mantle melting: application to volcanic arc petrogenesis. Geological Society of London, Special Publication, vol. 76, pp. 373–403.

Pearce, J.A., Peate, D.W., 1995. Tectonic implications of the composition of volcanic arc lavas. Annual Review of Earth and Planetary Sciences 23, 251–285.

Philpotts, A.R., Shi, J., Brustman, C., 1998. Role of plagioclase crystal chains in the differentiation of partly crystallized basaltic magma. Nature 395, 343–346.

Pineau, F., Shilobreeva, S., Kadik, A., Javoy, M., 1998. Water solubility and D/H fractionation in the system basaltic andesite-H_2O at 1250 °C and between 0.5 and 3 kbar. Chemical Geology 147, 173–184.

Pinkerton, H., Norton, G., 1995. Rheological properties of basaltic lavas at sub-liquidus temperatures: laboratory and field measurements on lavas from Mount Etna. Journal of Volcanology and Geothermal Research 68, 307–323.

Pinkerton, H., Stevenson, R.J., 1992. Methods of determining the rheological properties of magmas at sub-liquidus temperatures. Journal of Volcanology and Geothermal Research 3, 47–66.

Pride, M.J., 1985. Preliminary geological map of the Mount Skukum Volcanic Complex, 105D-2, 3, 4, 5. Exploration and Geological Services Division, Yukon, Indian and Northern Affairs Canada, Open File, 1:25 000 scale map.

Pride, M.J., 1988. Bimodal volcanism along the Tintina Trench near Faro and Ross River. Yukon Geology, Exploration and Geological Services Division, Yukon, vol. 2. Indian and Northern Affairs Canada, pp. 69–80.

Resnick, J., 2003. Petrogenesis of the Paleogene Sloko Lake Volcanic Complex, northwestern British Columbia and implications for early Tertiary magmatism in the Coast Plutonic Complex. M.Sc. thesis, McGill University, Montréal, Québec, Canada.

Reiners, P.W., Nelson, B.K., Ghiorso, M.S., 1995. Assimilation of felsic crust by basaltic magma: thermal limits and extents of crustal contamination of mantle-derived magmas. Geology 23 (6), 563–566.

Roddick, J.A., 1983. Geophysical review and composition of the Coast Plutonic Complex south of latitude 55° N. Circum-pacific plutonic terranes, Memoir, vol. 159. Geological Society of America, pp. 195–212.

Roscoe, R., 1953. Suspensions. In: Hermans, J.J. (Ed.), Flow Properties of Disperse Systems, pp. 1–38.

Rusmore, M.E., Woodsworth, G.J., 1991. Coast plutonic complex: a mid-Cretaceous contractional orogen. Geology 19, 941–944.

Saar, M.O., Manga, M., Cashman, K.V., Fremouw, S., 2001. Numerical models of the onset of yield strength in crystal-melt suspensions. Earth and Planetary Science Letters 187, 367–379.

Shaw, H.R., 1972. Viscosities of magmatic silicate liquids: an empirical method of prediction. American Journal of Science 272, 870–893.

Shi, S., Francis, D., Ludden, J., Frederiksen, A., Bostock, M., 1998. Xenolith evidence for lithospheric melting above anomalously hot mantle beneath the northern Canadian Cordillera. Contributions to Mineralogy and Petrology 131, 39–53.

Sigmarsson, O., Condomines, M., Fourcade, S., 1992. Mantle and crustal contributions in the genesis of recent basalts from off-rift zones in Iceland: constraints from Th, Sr and O isotopes. Earth and Planetary Science Letters 110, 149–162.

Sisson, T.W., Grove, T.L., 1993. Experimental investigations of the role of H_2O in calc-alkaline differentiation and subduction zone magmatism. Contributions to Mineralogy and Petrology 113, 143–166.

Souther, J.G., 1991. Volcanic regimes, chapter 14. In: Gabrielse, E.H., Yorath, C.J. (Eds.), Geology of the Cordilleran Orogen in Canada, Geology of Canada, vol. G-2. Geological Survey of Canada, pp. 457–490.

Sparks, R.S.J., 1978. The dynamics of bubble formation and growth in magmas: a review and analysis. Journal of Volcanology and Geothermal Research 3, 1–37.

Sparks, R.S.J., 1997. Causes and consequences of pressurization in lava dome eruptions. Earth and Planetary Sciences Letters 150, 177–189.

Sparks, R.S.J., Sigurdsson, H., Wilson, L., 1977. Magma mixing: a mechanism of triggering acid explosive eruptions. Nature 267, 315–318.

Spulber, S.D., Rutherford, M.J., 1983. The origin of rhyolite and plagiogranite in oceanic crust: an experimental study. Journal of Petrology 24, 1–25.

Stein, D.J., Spera, F.J., 1992. Rheology and microstructure of magmatic emulsions: theory and experiments. Journal of Volcanology and Geothermal Research 49, 157–174.

Singer, B.S., Myers, J.D., Frost, C.D., 1992. Mid-Pleistocene lavas from Seguam volcanic centre, central Aleutian arc: closed-system fractional crystallization of a basalt to rhyolite eruptive suite. Contributions to Mineralogy and Petrology 110, 87–112.

Taylor, S.R., McLennan, S.M., 1995. The geochemical evolution of the continental crust. Reviews in Geophysics 33, 241–265.

Tatsumi, Y., Eggins, S., 1995. Subduction Zone Magmatism. Blackwell, Cambridge. 211 pp.

Tatsumi, Y., Nakashima, T., Tamura, Y., 2000. The petrology and geochemistry of calc-alkaline andesites on Shodo-Shima island, SW Japan. Journal of Petrology 43, 3–16.

Tempelman-Kluit, D.J., 1974. Reconnaissance geology of Aishihik Lake, Snag and part of Stewart River map-areas, west-central Yukon (115H, 115K-J and 115N-O). Geological Survey of Canada, Paper 73-41, p. 97 (includes Maps 16-1973, 17-1973, 18-1973, 1: 250 000 scale).

Tempelman-Kluit, D.J., Currie, R., 1978. Reconnaissance rock geochemistry of Aishihik Lake, Snag and Stewart River map-areas in the Yukon crystalline terrane. Paper, vol. 77-8. Geological Survey of Canada. 72 pp.

Tepper, J.H., Nelson, B., K., Bergantz, W., Irving, A.J., 1993. Petrology of the Chilliwack Batholith, North Cascades

Washington: generation of calc-alkaline granitoids by melting of mafic lower crust with variable water fugacity. Contributions to Mineralogy and Petrology 113, 333–351.

Thompson, A.B, Matile, L., Ulmer, P., 2002. Some thermal constraint on crustal assimilation during fractionation of hydrous, mantle-derived magmas with examples from Central Alpine batholiths. Journal of Petrology 43 (3), 403–422.

Tuttle, O.F., Bowen, N.L., 1958. Origin of granite in the light of experimental studies in the system $NaAlSi_3O_8$–$KAlSi_3O_8$–SiO_2–H_2O. Memoir, vol. 74. The Geological Society of America. 153 pp.

Valley, P.M., Whitney, D.L., Paterson, S.R., Miller, R.B., Alsleben, H., 2003. Metamorphism of the deepest exposed arc rocks in the Cretaceous to Paleogene Cascades belt, Washington: evidence for large-scale vertical motion in a continental arc. Journal of Metamorphic Geology 21, 203–220.

Wen, S., Nekvasil, H., 1994. Solvcalc: an interactive graphics program package for calculating the ternary feldspar solvus and for two-feldspar geothermometry. Computers & Geosciences 20, 1025–1040.

Wickham, S.M., 1987. The segregation and emplacement of granitic magmas. Journal of the Geological Society (London) 144, 281–297.

Wheeler, J.O., McFeely, P., 1991. Tectonic Assemblage Map of the Canadian Cordillera and adjacent parts of the United States of America., Geological Survey of Canada, Map 1712A, 1: 1000000 scale.

Whitney, D.L., Miller, R.B., Paterson, S.R., 1999. P-T-t evidence for mechanisms of vertical tectonic motion in a contractional orogen: north-western US and Canadian Cordillera. Journal of Metamorphic Geology 17, 75–90.

Wyllie, P.J., 1963. Effects of the changes in slope occurring on liquidus and solidus paths in the system diopside–anorthite–albite. Mineralogical Society of America Special Publication 1, 204–212.